Doctoral Dissertation

Study on the progression of human embryonal rhabdomyosarcoma in the cell sheet system

Menglu Li

April 2017

Graduate School of Engineering

Osaka University

Contents

Chapter 1 General introduction

1.1 Rhabdomyosarcoma

Rhabdomyosarcoma (RMS), a type of cancer in which tumor cells are thought to arise from skeletal muscle, is the most common soft tissue sarcoma found in children (Hettmer and Wagers, 2010). There are two main types of RMS based on their histopathological features: the embryonal RMS (ERMS) which comprising 80% of RMS, and alveolar RMS (ARMS) with a worse overall outcome (Merlino and Helman, 1999; Parham, 2001; Zhu and Davie, 2015). ARMS is characterized by t(2;13)(q35;q14) or t(1;13)(q36;q14) translocations, which creates the novel PAX3-FOXO1 or PAX7-FOXO1 fusion proteins. Loss of heterozygosity of chromosome 11p15.5 and chromosome gains (chromosome 2, 8, 12, 13) are frequently detected in ERMS (Anderson *et al.*, 1999).

The current treatments for RMS patients include surgery, radiotherapy and combinations of conventional chemotherapeutic drug, such as vincristine and dactinomycin (VA treatment). These multimodal treatments have increased overall survival in patients with localized RMS to more than 80%. However, most RMS tumors are systemic cancers with both localized tumor lesion and distant spread of cancer cells. Approximately one in five RMS patients are diagnosed initially with metastatic diseases (Parham, 2001; Wexler, 2015). Outcome for patients diagnosed with metastatic disease remains poor below 30% (Belyea *et al.*, 2012; Dantonello *et al.*, 2011). Metastatic disease is a major cause to death in primary and relapsed RMS (Oberlin *et al.*, 2008; Wexler, 2015). As RMS is always diagnosed with metastasis, one critical problem is failure to acquire adequate information of primary tumor. It remains largely unknown what is the tissue microenvironment at the primary site, how does this tumor differentiate and

develop to a malignant one, which specific oncogenic events acquired during tumor progression. These problems hindered the progress in RMS research.

1.2 Tumor progression and metastasis

Tumor progression is a complex procedure with an accumulation of genetic alterations caused by genetic factors or external factors, such as physical carcinogens, chemical carcinogens and biological carcinogens (Yokota, 2000). There are two important status in the process of tumor progression, including primary tumor and metastatic tumor (**Figure 1-1**). In the state of primary tumor, tumor cells were restricted in a limited area with low oxygen and nutrients supply. A benign tumor can exist in patients for many years without causing damages to the body. After diagnosis, this primary tumor can be easily treated by surgery or radiotherapy. The worst case is a malignant one. Cells in these tumors acquire more genetic mutations, migrating away from their original site, invading nearby normal tissues and spreading to other parts of the human body, which makes cancer a life-threatening disease.

Tumor malignancy begins with invasion into surrounding environment, followed by new blood vessel formation toward tumor core and spread to other parts of the body using circulation system (van Zijl *et al.*, 2011). Tumor growth is accompanied by increasing pressure to its surrounding environment, while the surrounding tissue fights against the tumor growth via increasing pressure on tumor cells, such as increased interstitial pressure, hypoxia conditions and recruiting immune cells (Krakhmal *et al.*, 2015). Some tumor cells are subjected to apoptosis and make a necrosis core in tumor mass. However, some more “rogue” tumor cells gain an aggressive phenotype and the ability to metastatic progression. Tumor invasion is enabled by the detachment of tumor cells from the original

tumor mass due to downregulating intercellular adhesion molecules. Therefore, the cells gain the ability of high motility to enter the surrounding environment. Assisting by the elevated expression of matrix metalloproteinases (MMPs) to digest extracellular matrix (ECM), tumor cells invade into the surrounding tissue and remodel their surrounding environment to pave the way for migration.

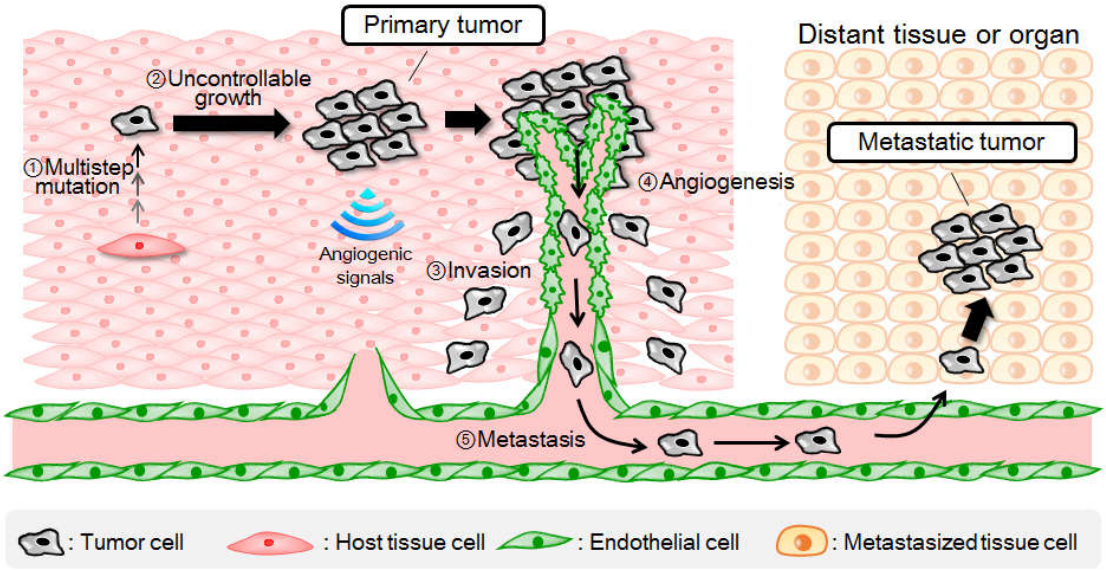

Figure 1-1 Tumor progression and metastasis.

Angiogenesis is a normal and vital process in growth and development by which new blood vessels are formed to supply nutrients and oxygen for cells (Breier, 2000; Chung and Ferrara, 2011; Folkman, 2006). Normal human cells are located within 100 to 200 μm of blood vessels to obtain sufficient oxygen supply. However, tumor, which is originated from one transformed cell, cannot allow for proper vascularization to occur as it is a rapidly expanding mass. Therefore, tumor without vascularization will live in an environment of low oxygen and nutrition which restrict tumor size in 1-2 mm diameter. In order to break this living limitation, tumor should find its way to get oxygen and nutrition supply. One approach is to induce angiogenesis generated from existing blood

vessel nearby. Once tumor completes to reach the normal blood vessels, metastatic spread will occur thus a benign tumor will switch to a malignant one. Since it was proposed that new blood vessel formation was an essential procedure to switch on tumor metastasis, tumor angiogenesis has become a therapeutic target for the treatment of cancer (Folkman, 1971).

1.3 Conventional model system in RMS research

The urge to find effective therapies against RMS promotes the need to further investigate the molecular mechanisms of this malignancy. To deepen the understanding of RMS diseases, many model systems have been established to elucidate the mechanism and to develop new therapeutic strategies (Kashi *et al.*, 2015). The systems modeling RMS are categorized into *in vitro* cell-based systems and *in vivo* xenograft models. There are numerous RMS cell lines derived from patient tumor samples, including 18 embryonal and 12 alveolar RMS cell lines being used by many researches (Hinson *et al.*, 2013). Except for derived cell lines, genetically modified RMS cells have been also highlighted. Genetically modified cells are applied to uncover the genetic alterations in the initiation and progression of RMS tumor. Linardic *et al.*, created genetic modified RMS cells by introducing the T/t-Ag, hTERT and H-Ras transgenes into the human skeletal muscle cells (Linardic *et al.*, 2005). Animal model is an alternative method to understand tumor development and mechanism *in vivo*. ERMS and ARMS have been modeled in xenograft mouse model and genetically engineered mice and reported in many literatures (Fleischmann *et al.*, 2003; Keller *et al.*, 2004; Nanni *et al.*, 2003; Nishijo *et al.*, 2009). Drosophila melanogaster was only reported to model ARMS by introducing the PAX7-FOXO1 gene into the skeletal muscle (Avirneni-Vadlamudi *et al.*, 2012; Galindo

et al., 2006). Langenau *et al.* created a new transgenic coinjection methodology to induce KRAS into zebrafish and established an ERMS zebrafish model (Ignatius *et al.*, 2012; Langenau *et al.*, 2007; Langenau *et al.*, 2008).

Although both *in vitro* cell-based systems and *in vivo* animal models demonstrate an important role in deciphering the mechanism of RMS progression and accelerating the drug discovery process, disadvantages and pitfalls remained. For the conventional cell culture *in vitro*, rigid and flat culture surface is utilized and cells are cultured as single cell or confluent monolayer. Two-dimensional (2D) cell culture is easy for operation and scaling-up, comprising the majority of cell-based assay nowadays. However, almost all cells in the body are surrounded by other cells and ECM, facing a complex three-dimensional (3D) environment other than a simple 2D surface (Pampaloni *et al.*, 2007). The main problem of 2D culture is that it does not represent the reality in the real *in vivo* conditions. In the process of drug discovery, the screening of potential drugs begins with the 2D cell culture tests, then the selected drugs will be used in the subsequent animal tests and clinical trials (Edmondson *et al.*, 2014). However, the positive compounds screened by 2D tests always fail in the clinical trials, especially in Phase III trials, which is the most expensive phase of clinical development. Animal models conquer the main problem of 2D cell culture and provide a 3D *in vivo* environment without ethical concerns to understand the development of human tumor. However, animal models are limited in mimicking the complexity of human tumorigenesis (van der Worp *et al.*, 2010). To induce tumorigenesis, immune-deficient animals are often used which cannot translate the normal response of human immune systems against tumor (Price, 2001). Other problems of animal models are less reproductive and difficult to control variables. Therefore, it is necessary to establish novel models which more closely mimic the *in vivo* conditions with

easy operation method to fill the gap between 2D cell culture systems and *in vivo* animal models.

1.4 Cell sheet engineering

Cell sheet engineering is a novel approach to fabricate 3D tissue constructs without scaffold (Matsuda *et al.*, 2007; Yamato and Okano, 2004; Yang *et al.*, 2007). This is achieved by culturing cells on the temperature-responsive polymer grafted surface, such as poly-*N*-isopropylacrylamide (PNIPAAm), which was developed by Dr. Teruo Okano in Tokyo Women's Medical University (Okano *et al.*, 1995). Above 32ºC, the culture surface is hydrophobic to facilitate cell attachment and proliferation to form cell monolayer. Below 32ºC, the culture surface is hydrophilic to initiate detachment of the whole monolayer from the surface. By simply lowering the temperature, an intact monolayer preserving both cells and ECM can be harvested. Combining with stamp manipulation method (Haraguchi *et al.*, 2012), multilayered cell sheet can be fabricated.

Cell sheet technology has firstly demonstrated its potential in tissue transplantation. Epithelial sheet for corneal regeneration (Nishida *et al.*, 2004) and skeletal myoblast cell sheet for cardiac failure (Sawa and Miyagawa, 2013; Sawa *et al.*, 2015; Shimizu *et al.*, 2003) were constructed and applied in the clinical trials. In 2016, a product named HeartSheet was developed by Terumo Corporation and authorized for marketing in Japan (Sawa *et al.*, 2015). Not only in the field of tissue transplantation, cell sheet technology can also provide multicellular culture systems for *in vitro* studies. There are two main merits of cell sheets compared with other multicellular culture systems. Firstly, Cell sheets preserve both the cells and the naturally formed ECM, thus closely mimicking the true *in vivo* conditions (Yamato and Okano, 2004). Another advantage appeared in the

observation of cell behaviors. The observation of cell behaviors can be simply divided into the X-Y plane and the Z-axis, enabling temporal and spatial interpretation (Kino-oka *et al.*, 2012; Nagamori *et al.*, 2013). In our previous studies, multilayered human skeletal muscle myoblast (HSMM) sheet has been constructed and sheet fluidity was proposed to evaluate the quality of cell sheet (Kino-oka *et al.*, 2012). To mimic the process of angiogenesis after transplantation, HSMM sheet was co-cultured with endothelial cells and a quantitative analysis method was applied to understand the formation of endothelial network (Nagamori *et al.*, 2013; Ngo *et al.*, 2013).

Although cell sheet technology constitutes a novel technology to use in tissue engineering and *in vitro* model studies, there have been few applications of this technique in the cancer research field. To the best of our knowledge, the only cancer-related instance of cell sheet use was *in vivo* studies in which monolayer or multilayer of cancer cells were harvested and used to induce tumors in mice (Akimoto *et al.*, 2013; Suzuki *et al.*, 2014). Cell sheet technology will show more potential in the field of cancer research and drug screening.

1.5 Objective of this study

There is an increasing demand of more effective *in vitro* models for elucidation mechanism in the progression of RMS. To widen the knowledge of RMS progression, this study aimed at understanding tumor cell behaviors in the 3D mimicry system. The interest is focused on the important processes in tumor malignancy, including tumor cell migration, invasion into surrounding environment and tumor angiogenesis. Tumor specific phenomena were investigated in the multicellular culture system and provide novel knowledge in the progression of RMS.

1.6 Research outline

This thesis focuses on the study of RMS cell behaviors in the cell sheet system and represents the important processes in tumor progression (**Figure 1-2**). Firstly, RMS cell migration in myoblast sheet was investigated to understand the difference between tumor and host tissue cells. Secondly, heterotypic interactions among RMS cells and host tissue cells were studied to reveal the mechanism in tumor invasion. Finally, the effect of RMS cells on the behaviors of endothelial cells was investigated. This thesis consists of five chapters including general introduction (chapter 1) and concluding remarks (chapter 5).

Up-regulated migration is one hallmark of tumor cells. In chapter 2, migration ability of human embryonal RMS cells (RDs) was studied in the 3D human skeletal muscle myoblast (HSMM) sheet. The analysis of cell migration was divided into vertical migration and horizontal migration to understand migration in the 3D format.

After acquiring migration ability, tumor cells will invade their surrounding environment to seek a way out. In chapter 3, multilayered heterogeneous RD sheets were constructed by co-culturing HSMMs and RDs. Time-lapse observation was used to reveal the dynamics of tumor cells in the HSMM sheets. This study revealed heterotypic interaction of tumor cells with normal myoblasts in a 3D cell sheet model, and brought new insights into the RMS invasion.

Tumor angiogenesis is an important trigger of malignancy by providing oxygen and nutrients to the “starved” primary tumor. In chapter 4, green fluorescent protein expressing human umbilical vein endothelial cells (GFP-HUVECs) were co-cultured with tumor-containing cell sheet to understand the effect of tumor cells on endothelial behaviors. Unlike the conventional study of tumor angiogenesis, which focusing on the paracrine secreted from tumor cells, this chapter studied how the environment change

caused by a minor population of RDs affects endothelial network formation. The environment change as well as endothelial network formation was analyzed quantitatively in this chapter.

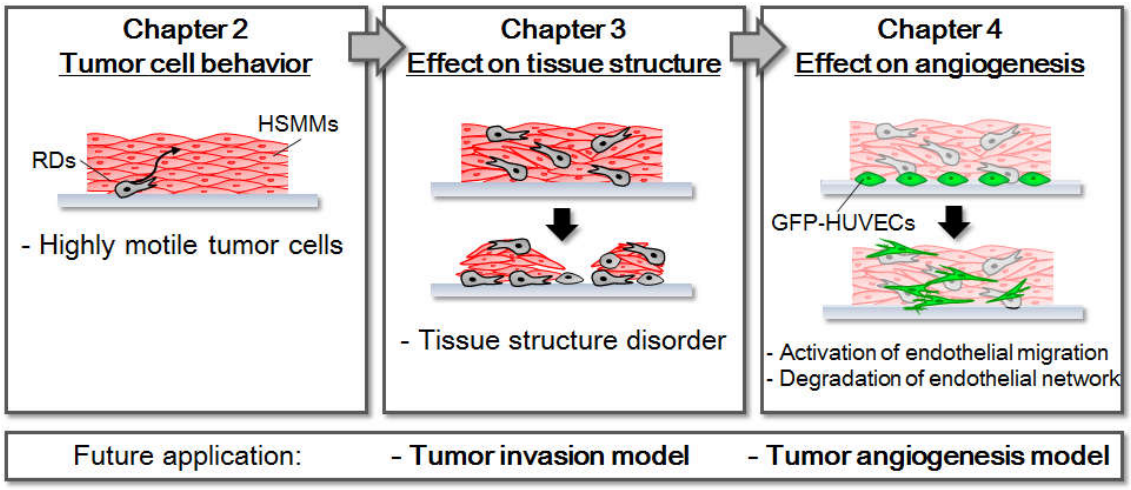

Figure 1-2 Outline of my PhD Thesis.

Chapter 2 Migratory behavior of RMS cells in multilayered myoblast sheet

2.1 Introduction

RMS is a tumor characterized by its high frequency to undergo metastasis (Masia *et al.*, 2012; Parham, 2001; Wang and Nicolson, 1983). One essential step to initiate tumor metastasis is local invasion into surrounding tissues. Invasive phenotype of tumor cells is always associated with higher migration properties, such as elevated MMPs secretion, abnormal expression of cell adhesion molecules and growth factor receptors. Understanding migratory behavior of RMS cells is necessary to investigate RMS progression.

Conventionally, cell migration has been investigated on 2D substrate or in 3D matrix (**Figure 2-1**). Many literatures already demonstrated that cell migration in 3D or *in vivo* was different from what we observed on 2D substrate due to less of one dimension (Baumann, 2012; Friedl *et al.*, 2012; Friedl *et al.*, 1998; Petrie and Yamada, 2012). For 3D matrix, although it provides a 3D playground for cell migration, lack of heterogenic cell contact limits its application in cancer research. 3D spheroid culture closely resemble the *in vivo* conditions. However, real-time tracking of individual cell cannot be realized in this system, only endpoint analysis can be performed. An alternative 3D multicellular model with quantitative analysis method is required.

Cell sheet consists of both cells and naturally formed ECM, which mimic the *in vivo* conditions. Quantitative analysis can be easily divided into components of the X-Y plane and the Z-axis, enabling its application in the study of cell migration. In our previous work, a five-layered HSMM sheet was fabricated as a 3D cell-based scaffold to study the

target cell behavior. Localization of human skeletal muscle fibroblasts (HSMFs) and GFP-HUVECs within a five-layered HSMM sheet was previously investigated (Nagamori *et al.*, 2013; Nagamori *et al.*, 2014; Ngo *et al.*, 2013). In this chapter, migratory behavior of RMS cells in five-layered HSMM sheet was investigated.

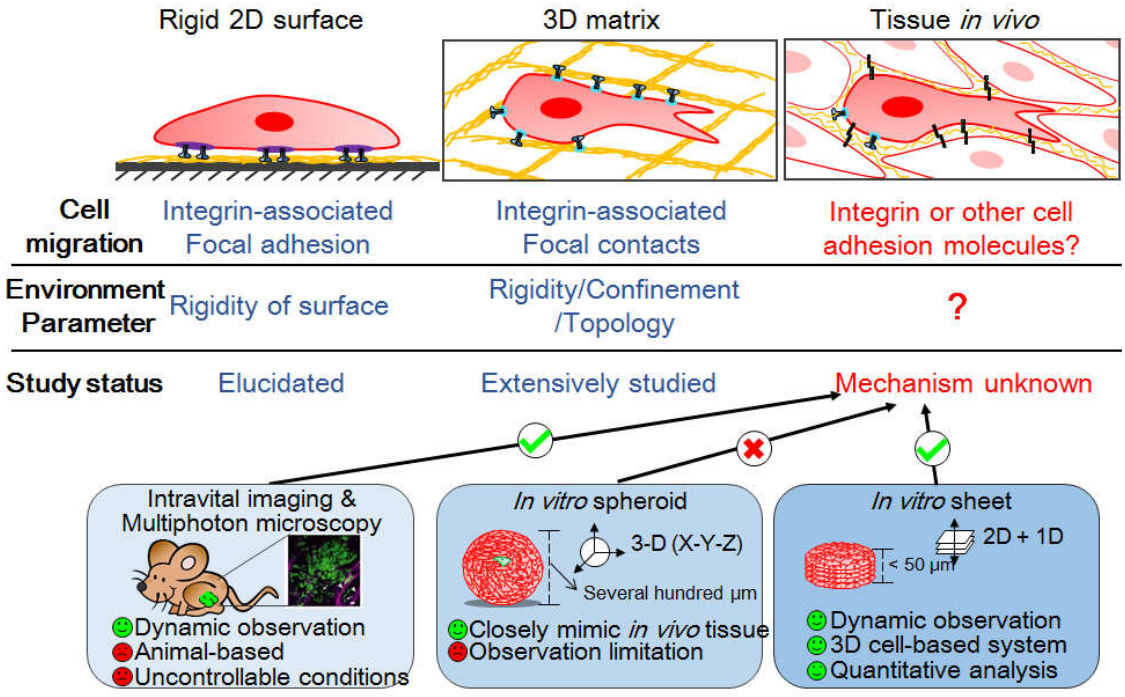

Figure 2-1 Summary of *in vitro* studies on cell migration.

2.2 Materials and methods

2.2.1 Cell preparation

Human skeletal muscle myoblasts (HSMMs, Lot. No. 4F1619; Lonza Walkersville Inc., Walkersville, MD) and a human ERMS cell line (RD, Cat. No. EC85111502, American Type Culture Collection, VA, USA) were used in this study. According to procedures described in our previous study (Nagamori *et al.*, 2013), subcultures of HSMMs on laminin-coated surfaces were conducted at 37°C in an atmosphere of 5% CO_2 in Dulbecco's Modified Eagle's Medium (DMEM; Sigma-Aldrich, MO, USA) containing 10% fetal bovine serum (FBS; ThermoFisher Scientific, MA, USA) and antibiotics (100 U/cm^3 penicillin G, 0.1 mg/cm^3 streptomycin, and 0.25 mg/cm^3 amphotericin B; Invitrogen, CA, USA). RDs were grown in the same medium as the HSMMs without laminin coating. The medium depth was set to 2 mm throughout the experiments. All cells were harvested until 70%–80% confluency.

2.2.2 Fabrication of five-layered cell sheet using stamping method

HSMMs harvested from subcultures were employed to fabricate five-layered cell sheet according to a previously developed method (Ngo *et al.*, 2013). HSMMs were seeded at 3.5×10^5 cells/cm^2 in each well of 24-well Upcell^{TM} plates (CellSeed, Tokyo, Japan) with a temperature-responsive PNIPAAm grafted surface and incubated for 24 h at 37°C in a 5% CO_2 atmosphere to form the monolayer sheet. The gelatin stamp was prepared by using a set of manipulators including jigs of a holder, metal stamps, a mold, a plunger, and a silicone rubber (**Figure 2-2 A**). A 7.5% (w/v) gelatin solution was prepared by dissolving gelatin powder from porcine skin (Sigma-Aldrich) in 5 ml Hank's balance salt solution (Sigma-Aldrich) with 100 µl 1N NaOH solution in 45°C water bath for 30

min. The solution was filtered through a 0.22-μm filter (Millex-GS; Millipore Co., Billerica, MA, USA) to be sterilized and poured into the mold, which was mounted on the silicone rubber in advance. The steal stamps were put onto the molds and the whole set was kept in 4°C refrigerator for 40 min to solidify the gelatin. The silicon rubber was removed and the mold was mounted onto the plunger to push out the gelatin stamps (**Figure 2-2 B**). 24-well temperature-responsive plate was put onto a heater plate with 37°C to avoid detachment. The gelatin stamp was overlaid on the monolayer sheet and the 24-well plate was transferred to incubate at 20°C for 30 min to harvest the monolayer sheet (**Figure 2-3**). Then the stamp was lifted together with the monolayer sheet and overlaid on another monolayer. This step was repeated to form the multilayered sheet. Using the plastic cap, the stamp as well as the multilayered sheet was transferred to the center of a 35-mm dish (ibidi GmbH, Martinsried, Germany). After incubation at 20°C for 2 h, the cell sheet was incubated at 37°C in the DMEM medium containing 10% (v/v) FBS for 1 h to remove the gelatin. The medium containing the dissolved gelatin was replaced with fresh medium. The medium was renewed every day.

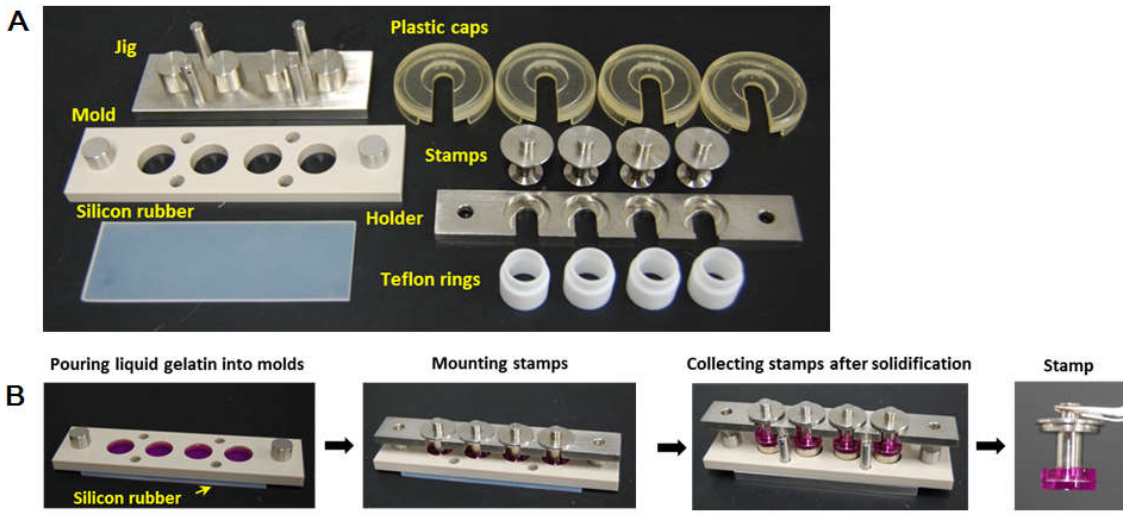

Figure 2-2 Manipulator set (A) and the preparation process of gelatin stamp (B).

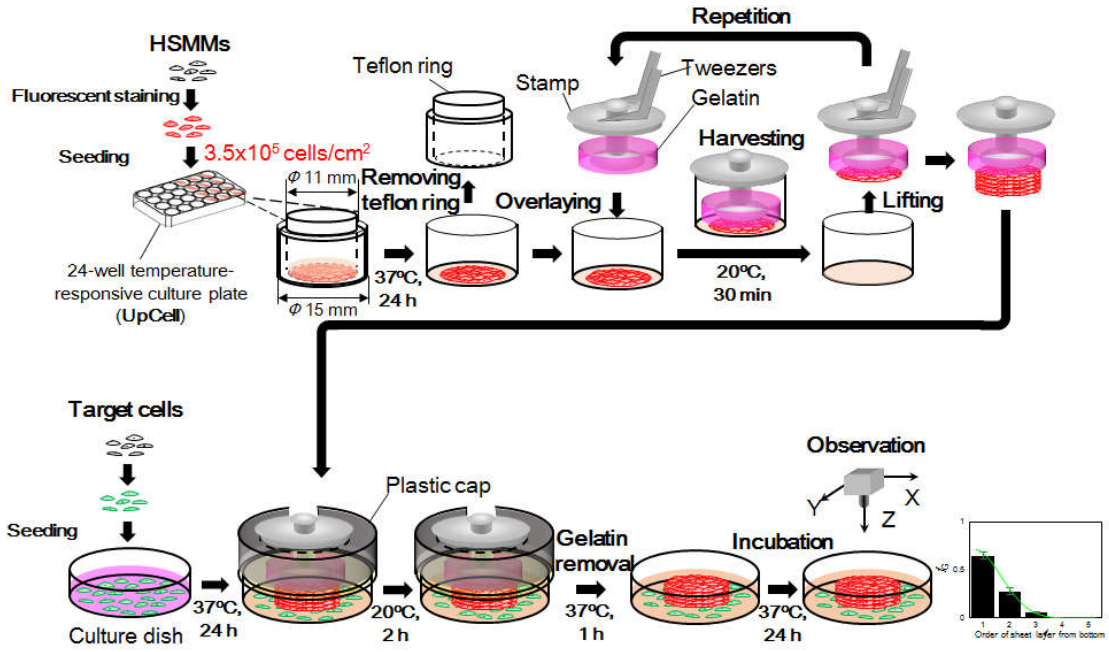

Figure 2-3 The procedure for stacking multilayered cell sheets and co-culturing with target cells.

2.2.3 Co-incubation of target cells with cell sheet

A five-layered HSMM sheet (stained using CellTracker™ Orange, Invitrogen) was fabricated and overlaid onto a 35-mm culture dish (ibidi GmbH) with the pre-cultured target cells (RDs or HSMMs), as shown in **Figure 2-4 A**. The target cells (stained using CellTracker™ Green, Invitrogen) seeded at 2.0×10^3 cells/cm^2 (Low density) and 2.0×10^4 cells/cm^2 (High density) were cultured in DMEM medium containing 10% (v/v) FBS for 24 h in advance. Time-course observation was conducted to understand cell morphology using a fluorescence microscope (IN Cell Analyzer 2000, GE Healthcare, BUX, UK). The samples were fixed using 4% paraformaldehyde (Wako Pure Chemical Industries, Osaka, Japan) at 24 h.

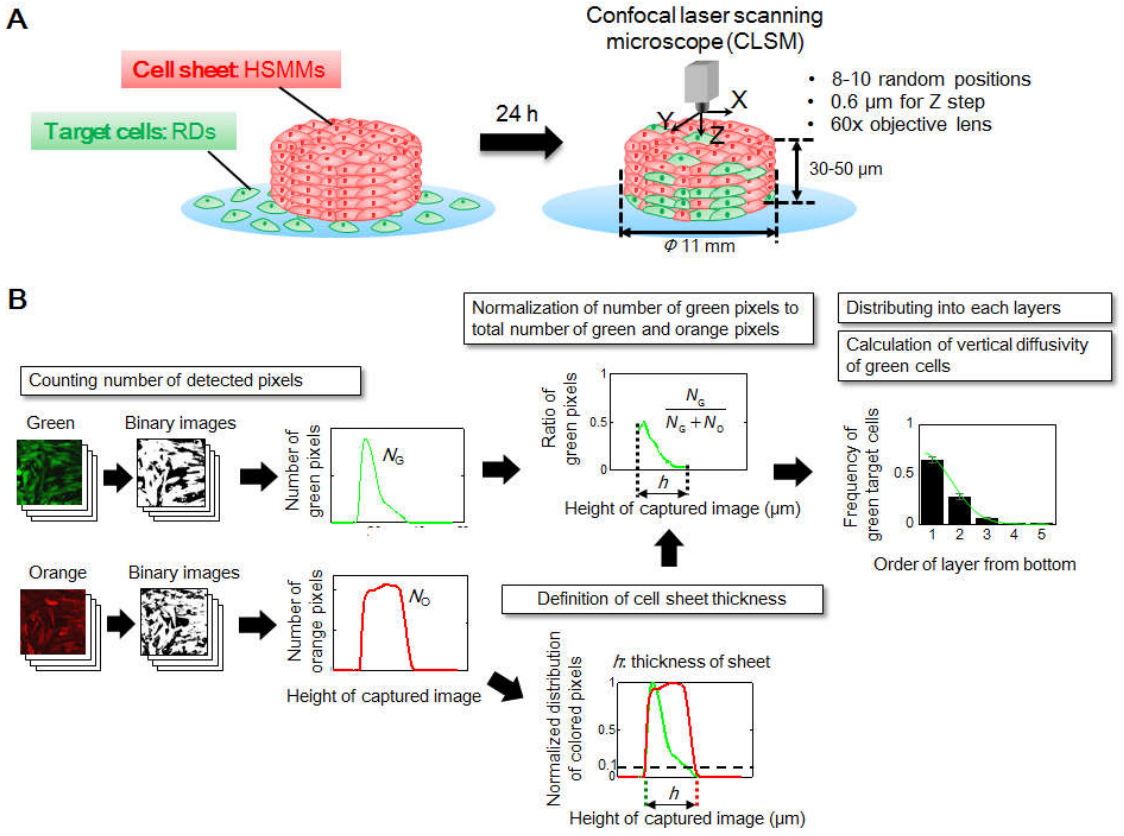

Figure 2-4 Analysis of vertical distribution of target cells. (**A**) Schematic drawing of experimental procedure. (**B**) Quantitative analysis method with image processing.

2.2.4 Vertical distribution of target cells in HSMM sheet

The vertical distribution of the green target cells within the HSMM sheet was observed by a confocal laser scanning microscope (FV1000, Olympus, Tokyo, Japan) with a 60× objective lens at 9 random positions in each sample (Kino-oka *et al.*, 2012). Quantitative analysis method with image processing was shown in **Figure 2-4 B**. Original 8-bit images (256×256 pixels) of both colors in each slice were converted into binary images after identifying intensity threshold values. The ratio of green pixels to sum of green pixels in each slice was normalized to determine the distribution of green pixels by dividing into five layers. The normalized distribution of green pixels was assumed to be equivalent to the green cell distribution in the sheet, which was considered to be the frequency of green cells, f_G, in each layer. To quantify sheet fluidity, the *diffusivity* (D, $\mu m^2/h$) was applied to measure vertical distribution of target cells based on Fick's second law, $\frac{\partial f_G}{\partial t} = D\frac{\partial^2 f_G}{\partial h^2}$, in which f_G, t and h represent the green cell frequency, incubation time, and sheet thickness, respectively. The Crank-Nicolson finite difference method and least squares method were applied to calculate the diffusivity using a customized software designed by LabVIEW (National Instruments, Austin, TX, USA).

2.2.5 Horizontal migration rate of target cells in HSMM sheet

To estimate the horizontal migration of target cells in HSMM sheet, a HSMM monolayer sheet including 0.5% of target cells stained with a fluorescence regent (CellTracker^{TM} Green, Invitrogen) was placed in the 3rd layer of a five-layered HSMM sheet. Time-lapse images were captured every 20 min using a fluorescence microscope (IN Cell Analyzer 2000, GE Healthcare) with a 10× objective lens (**Figure 2-5 A**).

Captured images at each time points were subjected to image processing using a customized software designated by LabVIEW (National Instruments) as previously described (Kino-oka *et al.*, 2004). The centroids (x_i, y_i) of each cell at each time point were determined (**Figure 2-5 B**). To calculate the average horizontal migration rate (V, μm/h) of target cells, the sum of cell displacement during each time interval was divided by the overall culture time. The observation was carried out for 10 h at 20 min interval.

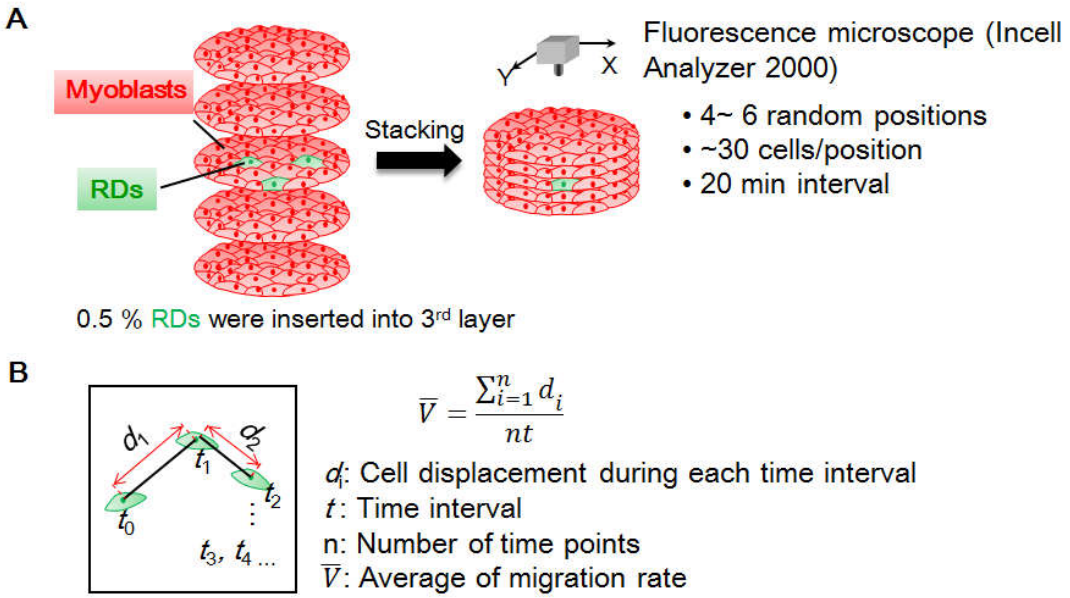

Figure 2-5 Analysis of horizontal migration rate in cell sheet.
(**A**) Schematic drawing of experimental procedure. (**B**) Analysis method.

2.2.6 Statistical analysis

Data presented in this study were obtained from three independent cultures and expressed as means with standard deviations (SDs). Student's t-test was used to determine the statistical significance of differences among data sets, and values of $P < 0.05$ were considered significant.

2.3 Results

2.3.1 Vertical distribution of target cells in HSMM sheet

To understand the migration pattern of RDs in HSMM sheet, two densities were set to reach single cell state and confluent state. Condition of confluent state was designed to evaluate whether cellular connection among RDs would affect their vertical migration pattern. The initial density of RDs was $0.23 \pm 0.02 \times 10^4$ cells/cm^2 and $3.39 \pm 0.47 \times 10^4$ cells/cm^2 at low and high seeding condition, respectively. The initial density of control HSMM was $0.21 \pm 0.02 \times 10^4$ cells/cm^2 in low seeding density and $2.79 \pm 0.17 \times 10^4$ cells/cm^2 in high seeding density, respectively.

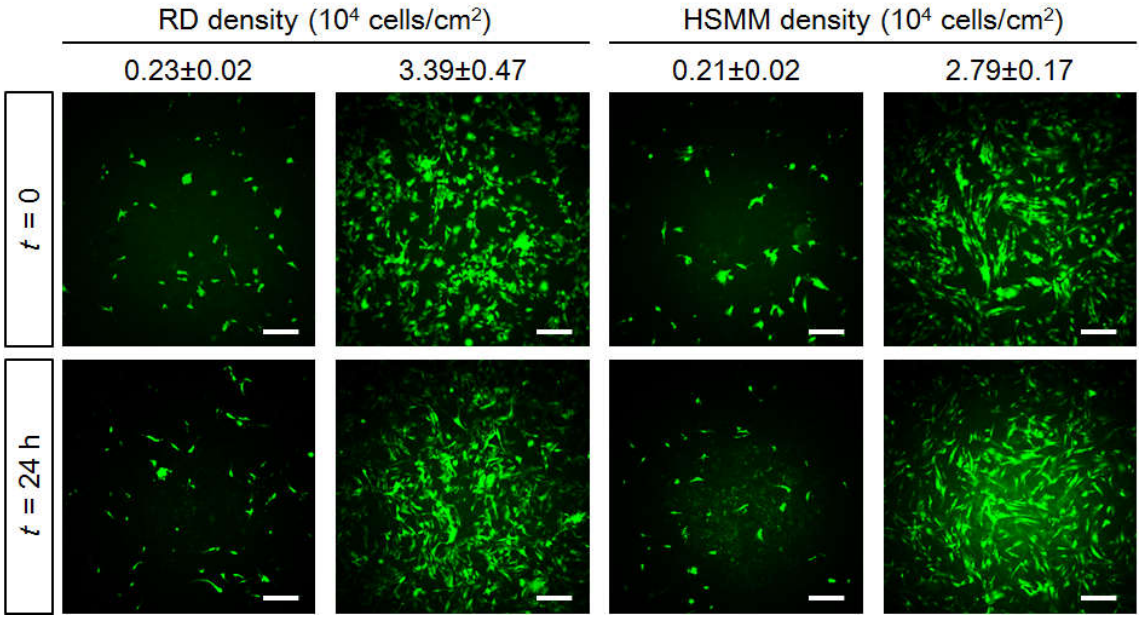

Figure 2-6 Morphology of target cells at $t = 0$ and $t = 24$ h. Scale bar: 200 μm.

Cellular morphology was observed within 24 h culture time. In the case of low density, RDs showed stretched morphology at initial time and stared to elongate at $t = 24$ h similar to HSMMs. In the case of high density, RDs and HSMMs showed stretched morphology in confluent state at $t = 0$ (**Figure 2-6**). After culturing for 24 h, all the cells

showed elongated cell morphology without formation of network (Nagamori *et al.*, 2013) or aggregation (Nagamori *et al.*, 2014) which indicated that RDs and myoblasts migrate randomly.

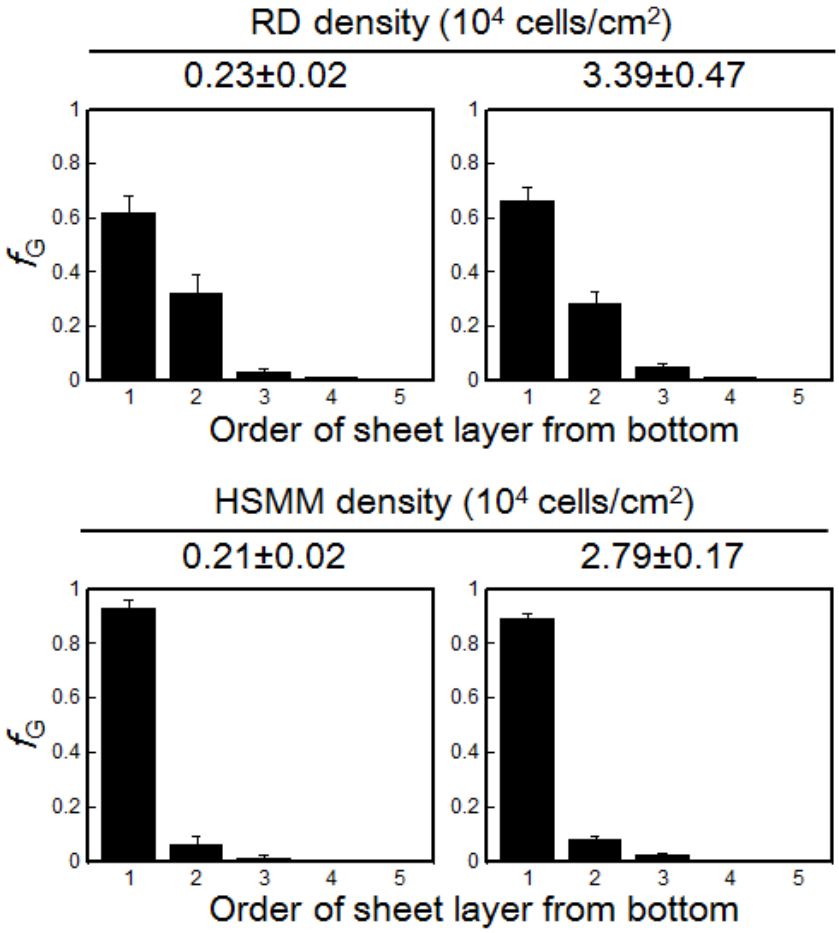

Figure 2-7 Vertical distribution of target cells in HSMM sheet at t = 24 h. Bars show standard deviation (SD) (n = 3).

After culturing for 24 h, vertical distribution and diffusivity were calculated to understand vertical migration of target cells quantitatively. Most RDs stayed in the first and second layer with the f_G value of 0.63 and 0.32 at low density and 0.66 and 0.28 at high density; while most myoblasts stayed in the first layer with the f_G value of 0.93 in the case of low density and 0.89 in the case of high density (**Figure 2-7**). It was found

that vertical distribution of RDs and myoblasts was not density-dependent due to their similar distribution at both low and high seeding density. Cellular connection among RDs and myoblasts did not affect their vertical migration pattern. The value of diffusivity was calculated based on the vertical distribution of target cells, diffusivity of RDs was 0.96 μm/h^2 and 0.95 μm/h^2 at low and high seeding density, which was about 5.5 and 9.5 times higher than that of myoblasts, demonstrating enhanced migration of RDs compared with HSMMs (**Figure 2-8**).

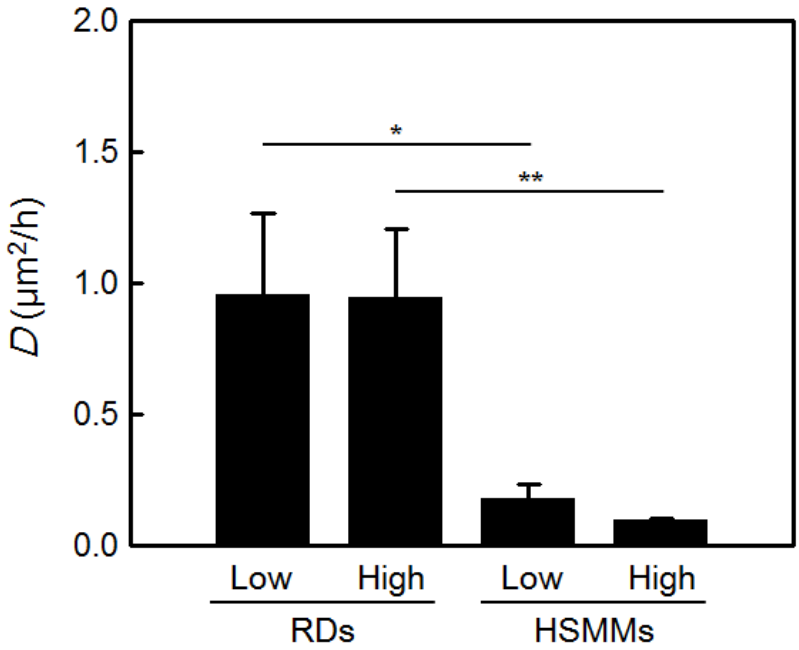

Figure 2-8 Diffusivity of target cells at different initial densities. Bars show standard deviation (SD) (n = 3). Asterisk indicates significant difference (*: $P < 0.05$, **: $P < 0.01$).

2.3.2 Horizontal migration rate of RDs in HSMM sheet

Horizontal migration rate of RDs in HSMM sheet was compared with HSMMs in HSMM sheet (**Figure 2-9**). 0.5% of RDs or HSMMs were stained green and tracked by a fluorescence microscopy with a 10× objective lens every 20 min. Migration rate of RDs and HSMM was calculated and the value were 7.35 μm/h and 5.07 μm/h, respectively.

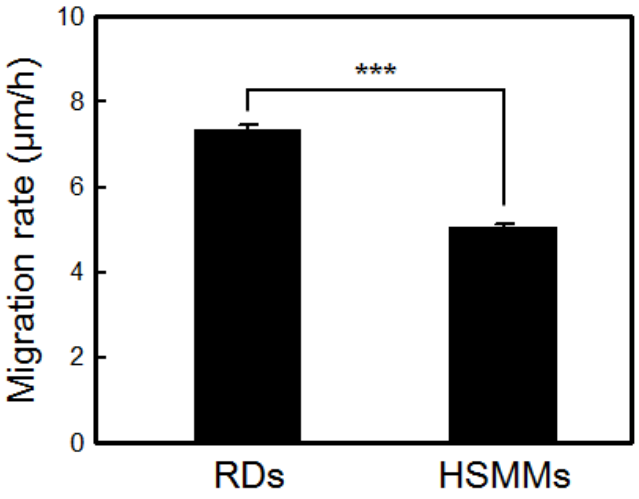

Figure 2-9 Horizontal migration rate of target cells in the 3rd layer of HSMM sheet. Bars show standard deviation (SD) (n = 3). Asterisk indicates significant difference (***: $P < 0.001$).

2.4 Discussion

In this chapter, migratory behavior of RDs was studied in a five-layered HSMM sheet by co-culturing RDs with HSMM sheet. Cell migration was quantified by dividing into vertical and horizontal direction to understand migration in a 3D format. Vertical migration of RDs was quantified based on the vertical distribution of RDs in each layer of cell sheet from the bottom to top. It was found that more RDs located towards the upper layer of cell sheet, demonstrating that RDs migrate faster in vertical direction compared with myoblasts (**Figure 2-7**). Horizontal migration of target cells was tracked by time-lapse observation and migration rate of RDs was calculated to be 7.35 μm/h, which is 1.5 times faster than that of myoblasts (5.07 μm/h) (**Figure 2-9**). RDs demonstrated a fast migratory phenotype compared with surrounding myoblasts both in vertical and horizontal direction.

Multilayered myoblast sheets consist of both cells and naturally formed ECM, providing a 3D playground to facilitate cell migration. Myoblast sheets have already been applied to understand target cell behaviors in our laboratory, including myoblasts, fibroblasts and HUVECs. Myoblasts were found migrate randomly and make cell sheet a homogeneous cell mixture with sheet fluidity (Kino-oka *et al.*, 2012). Fibroblasts quickly localize to the top layer of cell sheet in single cell state while form aggregates at the bottom layer in confluent state (Nagamori *et al.*, 2014). Endothelial cells undergo morphological change and form network at the proper seeding density (Nagamori *et al.*, 2013). To understand the different behavior of target cells in multilayered cell sheet, it is necessary to know the different adhesion molecules on the surface of each cell. Cadherin super-family is an important group of cellular adhesion molecules which mediate heterogeneous localization of cells in the 3D structure (Duguay *et al.*, 2003). N-cadherin

and M-cadherin were found expressed in human myoblasts in which N-cadherin is associated with myoblast migration and M-cadherin plays an important role in the fusion of myoblast (Kaufmann *et al.*, 1999; Wrobel *et al.*, 2007). In the myoblast sheet, connection mediated by N-cadherin and M-cadherin is balanced. Therefore, no specific localization of myoblast was observed. As a type of mesenchymal cell, fibroblasts express N-cadherin which mediated fibroblast migration in the myoblast sheet (Matsuyoshi and Imamura, 1997). However, it also reported that fibroblasts expressed OB-cadherin to form strong connection in high-density culture (Pittet *et al.*, 2008). VE-cadherin and N-cadherin are expressed in endothelial cells in which VE-cadherin mediated endothelial cell tube formation (Bach *et al.*, 1998; Kiran *et al.*, 2011). It suggested that different cellular adhesion molecules were accounted for the different cell behavior and localization in the cell sheet.

Abnormal expression and dysfunctional localization of N-cadherin and M-cadherin in the cellular contact sites were found in RMS cells (Charrasse *et al.*, 2004; Soler *et al.*, 1993). The possible mechanism of active RD migration within an HSMM sheet was considered as follows: unlike HSMMs, which are capable of strongly adhering to their own cell type, RDs formed weak adhesions to the surrounding HSMMs. Therefore, RDs can detach easily from previous connections and anchor to other adhesion sites to initiate fast migration.

2.5 Summary

Migratory behavior of RDs was investigated and quantified in cell sheet system. Compared with surrounding myoblast, RDs demonstrated a fast migratory phenotype both in vertical and horizontal direction. High motility, one hallmark of cancer, was represented in this *in vitro* model.

Chapter 3 Heterotypic interaction between RMS cells and host tissue cells

3.1 Introduction

After acquiring rapid migratory ability by abnormal expression of adhesion molecules and up-regulation of MMPs, tumor cells will face a microenvironment consists of ECMs and the cells that beget them, such as fibroblasts and host tissue cells (Friedl and Alexander, 2011). Cell-cell interaction, especially which between invasive tumor cells and normal cells, plays a vital role in tumor invasion and metastasis (Tisdale, 2004). Understanding heterotypic cellular interactions is beneficial for deciphering the mechanism of tumor invasion.

Conventionally, heterotypic cellular interaction has been investigated using 2D substrates or 3D ECM systems with or without direct contact. However, the playground to support cellular interaction *in vivo* is always through use of other cells (Bogdanowicz and Lu, 2013; Chandrasekaran *et al.*, 2012; Charras and Sahai, 2014). Intravital microscopy associated with multiphoton microscopy benefits real-time tracking of fluorescent human tumor cell in model animals; however, a gap still remains between animal models and real conditions in human body (Condeelis and Segall, 2003; Jain *et al.*, 2002). Human cells cultured as spheroid aggregates closely resemble *in vivo* solid tumors in terms of cellular heterogeneity, nutrient and oxygen gradients, and cell-cell connections (Thoma *et al.*, 2014; Vinci *et al.*, 2012). Studies in which normal and malignant epithelial cells were co-cultured in spheroids demonstrated that malignant epithelial cells engulf normal epithelial spheres (Ivers *et al.*, 2014). However, individual cell behavior inside a spheroid cannot be monitored in real time simultaneously with the

bulk properties of the spheroid, thereby presenting a challenge in understanding cellular interactions.

Cell sheet technology has been emerged as a powerful tool not only in tissue engineering, but also in modeling individual cell behavior on a 3D scale (Matsuda *et al.*, 2007; Yang *et al.*, 2007). In this technology, intact monolayer cell sheets containing ECM are harvested and layered to construct a multilayered cell sheet. This system consists of both cells and ECM, thereby closely resembling *in vivo* conditions. Quantitative analysis can be easily divided into components of the X-Y plane and the Z-axis. Unlike spheroid aggregates, the dynamic status of overall cell sheets can be estimated in terms of sheet fluidity (Kino-oka *et al.*, 2012).

This chapter aimed to reveal the interaction between RMS tumor cells (RDs) and non-malignant myoblast cells using a 3D cell sheet culture. Multilayered heterogeneous ERMS sheets were constructed by co-culturing RDs with HSMMs. Time-lapse observation was used to reveal the dynamics of tumor cells in the HSMM sheets and the structure of heterogeneous cell sheets. This chapter revealed heterotypic interaction between tumor cells and normal cells in a 3D cell sheet model, and highlighted the value of using 3D cultures to analyze the dynamics of tumor cells.

3.2 Materials and methods

3.2.1 Cell preparation

Human skeletal muscle myoblasts (HSMMs, Lot. No. 4F1619; Lonza Walkersville Inc.) and a human ERMS cell line (RD, Cat. No. EC85111502, American Type Culture Collection) were used in this study. Subcultures of HSMMs on laminin-coated surfaces were conducted at 37°C in an atmosphere of 5% CO_2 in Dulbecco's Modified Eagle's Medium (DMEM; Sigma-Aldrich) containing 10% fetal bovine serum (FBS; ThermoFisher Scientific) and antibiotics (100 U/cm^3 penicillin G, 0.1 mg/cm^3 streptomycin, and 0.25 mg/cm^3 amphotericin B; Invitrogen). RDs were grown in the same medium as the HSMMs without laminin coating. The medium depth was set to 2 mm throughout the experiments. All cells were harvested until 70%–80% confluency.

3.2.2 Fabrication of heterogeneous tumor cell sheet

HSMMs and RDs harvested from subcultures were stained with a fluorescent reagent (CellTracker^{TM} Orange and Green, Invitrogen) to obtain different fluorescence according to the commercial instruction. Heterogeneous monolayers were prepared by mixing different ratios of RDs (0%, 10%, 25%, 50%, 75% and 100%) with HSMMs to make final seeding density of 3.5×10^5 cells/cm^2 in each well of 24-well Upcell^{TM} plates (CellSeed) with a temperature-responsive PNIPAAm grafted surface and incubated for 24 h at 37°C in a 5% CO_2 atmosphere to form the monolayer sheet (**Figure 3-1**). Five-layered heterogeneous sheets were fabricated and cultured at 37°C in a 5% CO_2 atmosphere. Cell sheet morphology was observed by an imaging system (IN Cell Analyzer 2000, GE Healthcare) with a 2× objective lens at 0 and 96 h of incubation time. The samples were fixed at 96 h and observed using a confocal laser scanning microscope (FV1000, Olympus)

with a 60× objective lens.

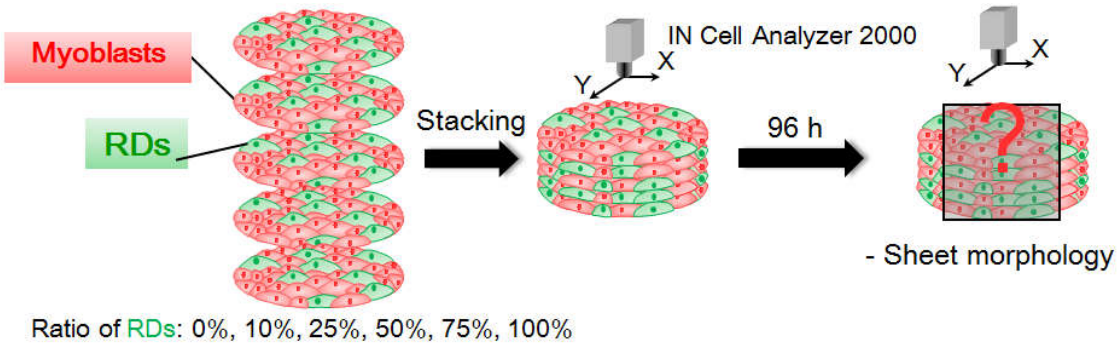

Figure 3-1 Fabrication of heterogeneous tumor cell sheet.

3.2.3 Evaluation of sheet fluidity in HSMM and RD sheet

Evaluation of sheet fluidity in the HSMM and RD sheets was based on a previously reported method (Kino-oka *et al.*, 2012). Briefly, a five-layered cell sheet with a basal layer (stained by CellTracker™ Green) and upper layers (stained by CellTracker™ Orange) was prepared to observe the spatial distribution of the basal target layer using a confocal laser scanning microscope (FV1000, Olympus) with a 60× objective lens at 9 random positions in each sample. Original 8-bit images (256×256 pixels) of both colors in each slice were converted into binary images after identifying intensity threshold values. The ratio of green pixels to sum of green pixels in each slice was normalized to determine the distribution of green pixels by dividing into five layers. The normalized distribution of green pixels was assumed to be equivalent to the green cell distribution in the sheet, which was considered to be the frequency of green cells, f_G, in each layer. To quantify sheet fluidity, the *diffusivity* (D, μm^2/h) was applied to measure vertical distribution of target cells based on Fick's second law, $\frac{\partial f_G}{\partial t} = D\frac{\partial^2 f_G}{\partial h^2}$, in which f_G, t and h represent the green cell frequency, incubation time, and sheet thickness, respectively.

The Crank-Nicolson finite difference method and least squares method were applied to calculate the diffusivity using a customized software designed by LabVIEW (National Instruments).

3.2.4 Spatial distribution of target cells in five-layered HSMM and RD sheet

To determine the vertical distribution of target cells (HSMMs and RDs) inside the HSMM and RD sheets, localization of the green target cells (HSMMs or RDs labeled green) within the red HSMM or RD sheets was observed by a confocal laser scanning microscope (FV1000, Olympus) with a 60× objective lens. Quantitative analysis of the frequency of green target cells and diffusivity is same as described above. Time-lapse observation was conducted to assess the dynamic behavior of individual cell by obtaining images every 1 h at several positions using a confocal laser scanning microscope (FV10i, Olympus).

3.2.5 Statistical analysis

Data presented in this study were obtained from three independent cultures and expressed as means with standard deviations (SDs). Student's t-test was used to determine the statistical significance of differences among data sets, and values of $P < 0.05$ were considered significant.

3.3 Results

3.3.1 Effect of RD ratio on sheet morphology disruption and segregation

To understand the effect of the RD ratio on the overall sheet structure, heterogeneous five-layered cell sheets were fabricated by stacking monolayer sheets with different ratios of RDs ranging from 0% to 100%. To visualize different cell types, RDs and HSMMs were stained green and red on captured images, respectively. **Figure 3-2A** depicts the morphologies of different heterogeneous cell sheets at the initial (t = 0) and final (t = 96 h) of the culture. At t = 0, all sheets were constructed with an intactly round shape, thereby demonstrating success in sheet fabrication. At t = 96 h, the sheets with low ratio of RDs (less than 50%) experienced destruction of overall sheet structure, while the sheets with high ratio of RDs (75% and even 100%) and HSMM control maintained their original shape and size. The sheet was found to be most disrupted when mixing 25% RDs into the HSMM sheet. After culturing for 96 h, samples were fixed to clarify the vertical localization of constituent cells. In the low RD ratio sheets (10% and 25%), HSMMs were surrounded by RDs as indicated by the white arrows in **Figure 3-2B**. Meanwhile, in the high RD ratio sheets (50%, 75%), individual HSMMs were found distributed in the upper layer of the cell sheets.

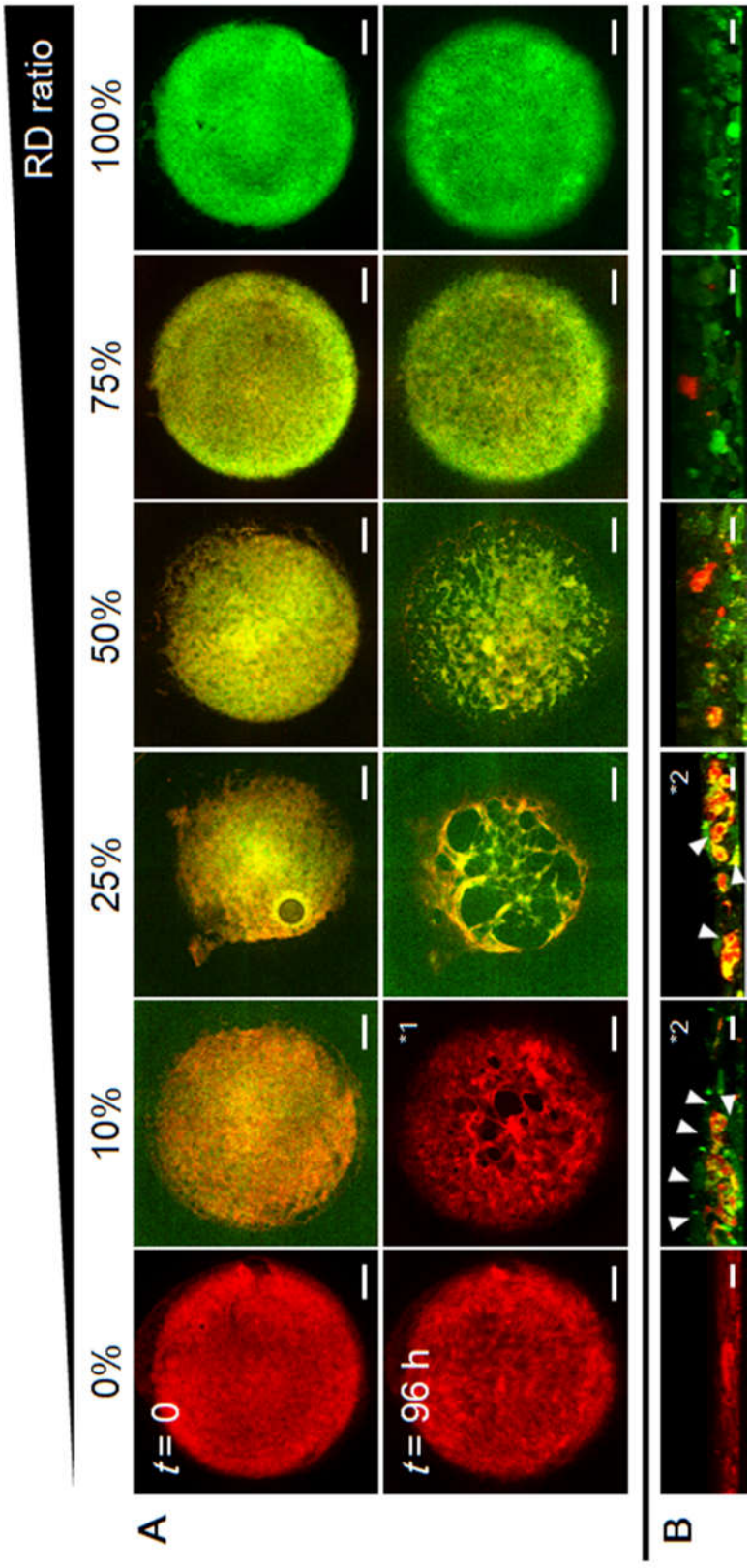

Figure 3-2 Effect of RD ratio on sheet structure deformation. (**A**) Time course of sheet morphology at $t = 0$ and 96 h. Scale bar: 2 mm. (**B**) Localization of RDs (green) and HSMMs (red) in heterogeneous sheets at 96 h. Arrows: RDs localized outside of HSMM aggregate. Scale bar: 20 μm. *1: Green channel was not combined due to weak fluorescence; *2: Contrast of green channel was enhanced to visualize RDs.

3.3.2 High sheet fluidity of RD sheet compared with HSMM sheet

The fluidity of RD sheets was compared with that of HSMM sheets. The basal layer of the cell sheet was stained to appear green on captured images as starter cells and upper layers were stained to appear red. After culturing for 24 h, the vertical distribution of the first layer of green cells was measured and sheet fluidity was calculated. Here, the thickness of HSMM sheet and RD sheet were 43.9 ± 0.5 μm and 78.3 ± 3.9 μm, respectively. **Figure 3-3A** shows the histogram of f_G in HSMM and RD sheets. In the HSMM sheet, the f_G value in the first and second layer from the bottom were estimated to be 0.80 and 0.19, respectively, while in the RD sheet, a broad distribution of 0.36, 0.28, and 0.21 was observed for the first, second and third layer, respectively. The vertical diffusivity of RDs, D, was estimated based on the Crank-Nicolson finite difference method and least squares method (**Figure 3-3B**), and had a value of 18.03 $\mu m^2/h$, which was about 56 times higher than that of the HSMM sheet ($D = 0.32$ $\mu m^2/h$).

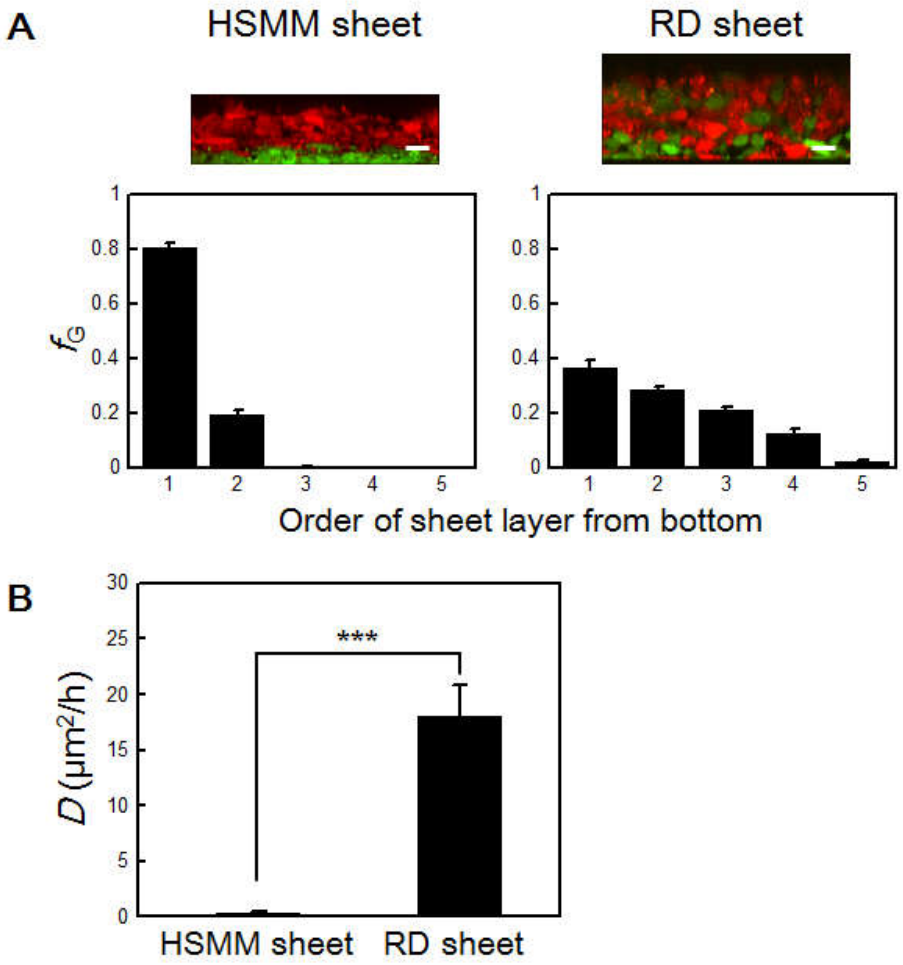

Figure 3-3 Evaluation of sheet fluidity in HSMM and RD sheets. (A) Frequency of the green cells (f_G) distributed in five layers inside the each sheet at t = 24 h. (B) Diffusivity of the HSMM and RD sheets. Bars show standard deviation (SD) (n = 3). Asterisk indicates significant difference (***: P < 0.001). Scale bar: 20 μm.

3.3.3 Vertical distribution of target cells in low and high fluidic sheet

Understanding single cell behavior in the lowest (HSMMs only) and highest (RDs only) fluidic sheets was beneficial to elucidating overall sheet deformation phenomenon. HSMM and RD sheets were fabricated and co-incubated with pre-cultured target cells (HSMMs and RDs) with a seeding density of 2.0 x 10^3 cells/cm^2. The distribution of target cells within the cell sheets was estimated and dynamic migration patterns were

monitored via time-lapse observation. **Figure 3-4A** shows the vertical distribution of target cells in HSMM and RD sheets at 24 h. Here, the thickness of HSMM and RD sheets were 38.3 ± 6.0 μm and 76.3 ± 5.3 μm, respectively. In the HSMM sheet, the f_G value of RDs in the first and second layer were 0.63 and 0.32, while 93% of HSMMs remained in the first layer. Surprisingly, when HSMMs and RDs were cultured in RD sheet, an elevated level of distribution was found. HSMMs distributed at a frequency of 0.66 and 0.30 in the first and second layer, similar to the distribution of RDs in the HSMM sheet, whereas RDs retained their migration potential and showed a broader distribution compared with HSMMs (**Figure 3-4A**). The value of diffusivity was calculated based on the vertical distribution of target cells, demonstrating that RDs had enhanced migration compared with HSMMs in both HSMM and RD sheets (**Figure 3-4B**). The dynamic behavior of RDs and HSMMs was monitored by confocal laser scanning microscopy, thereby revealing target cell migration patterns in HSMM and RD sheets, as shown in **Figure 3-5** and **Figure 3-6**. RDs underwent active migration in the HSMM sheet with one or more obvious leading pseudopods having a faster migration speed compared with surrounding HSMMs. Conversely, HSMMs possessed a spindle shape without pseudopods when surrounded by other HSMMs, demonstrating a restricted migration pattern (**Figure 3-5A**). The migration pattern of RDs in the RD sheet was same as that of the HSMM sheet with faster migration speed. In the RD sheet, HSMMs initially migrate with obvious pseudopods, but later migrated in a spherical shape with fewer pseudopods, thereby demonstrating failure in active migration (**Figure 3-5B**). Interestingly, HSMM aggregates were maintained in the HSMM sheet but disrupted in the RD sheet, which revealed that RDs can adversely affect myoblast interactions (**Figure 3-6**).

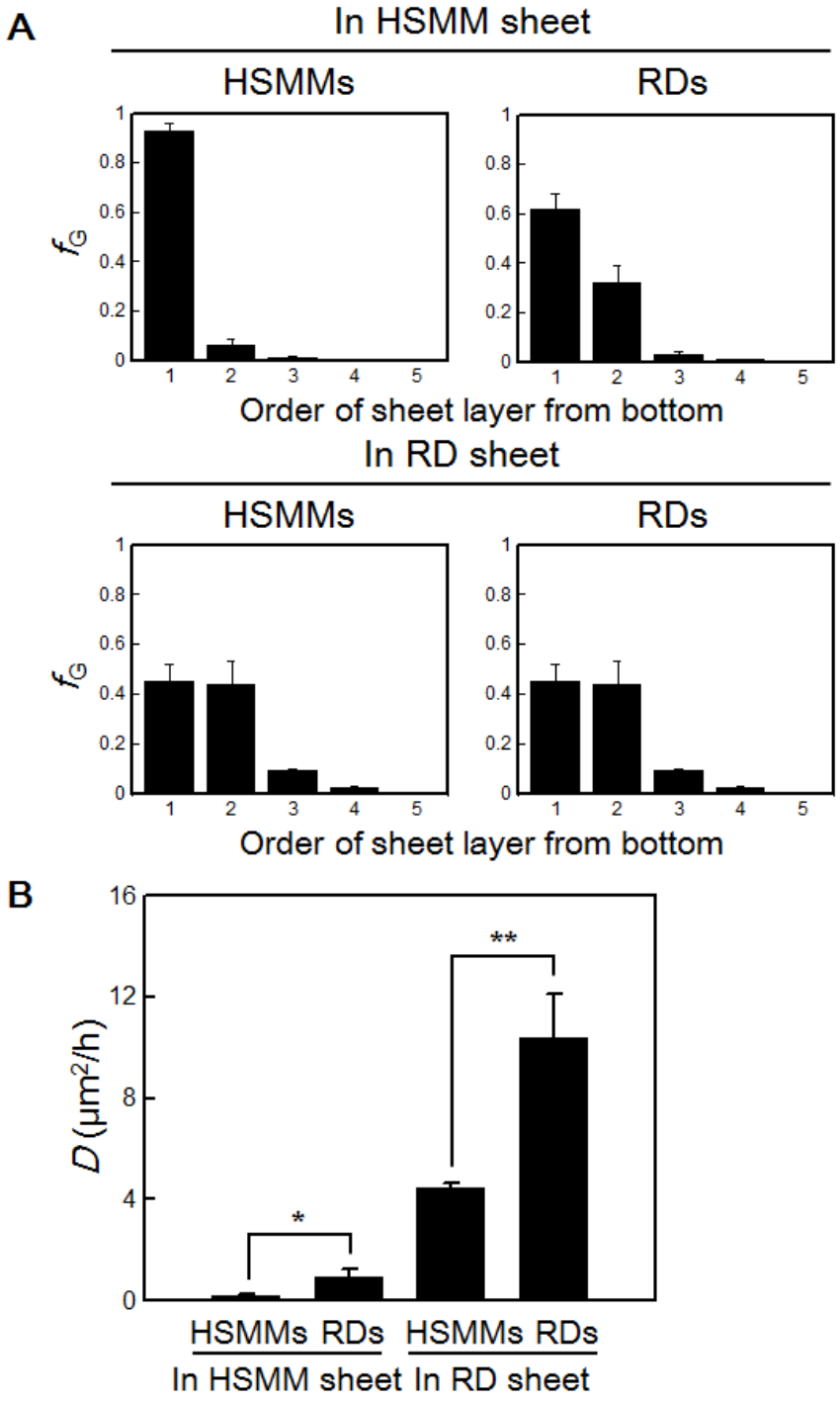

Figure 3-4 Vertical analysis of target cells inside the five-layered HSMM sheet or RD sheet. (**A**) Frequency of green target cells in each layer of HSMM or RD sheet. Bars show standard deviation (SD) (n = 3). (**B**) Diffusivity of target cells in different sheets. Bars show standard deviation (SD) (n = 3). Asterisk indicates significant difference (*: $P < 0.05$; **: $P < 0.01$).

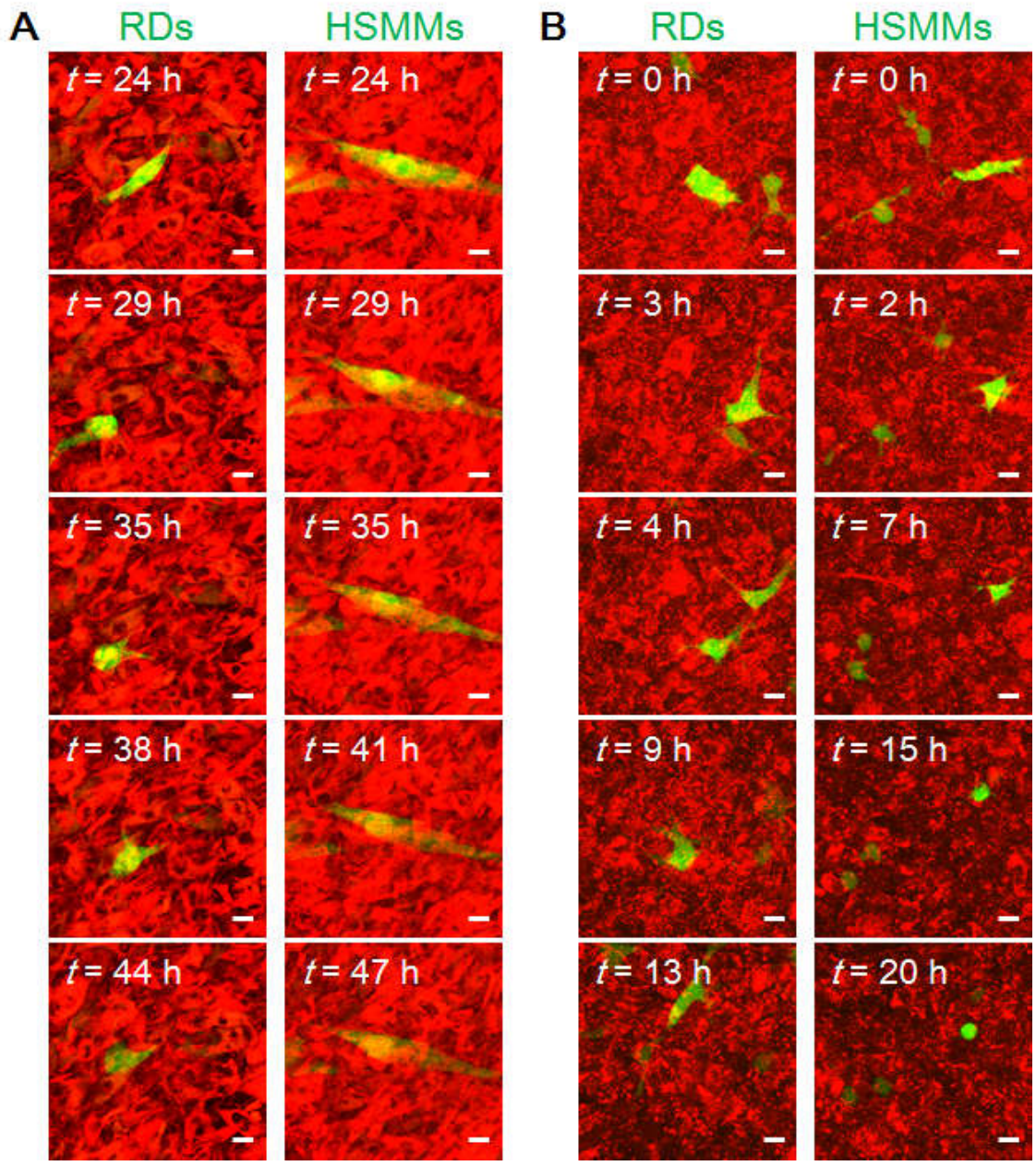

Figure 3-5 Time-lapse observation of target cells in HSMM sheet (**A**) and RD sheet (**B**) at low seeding density. Scale bar: 20 μm.

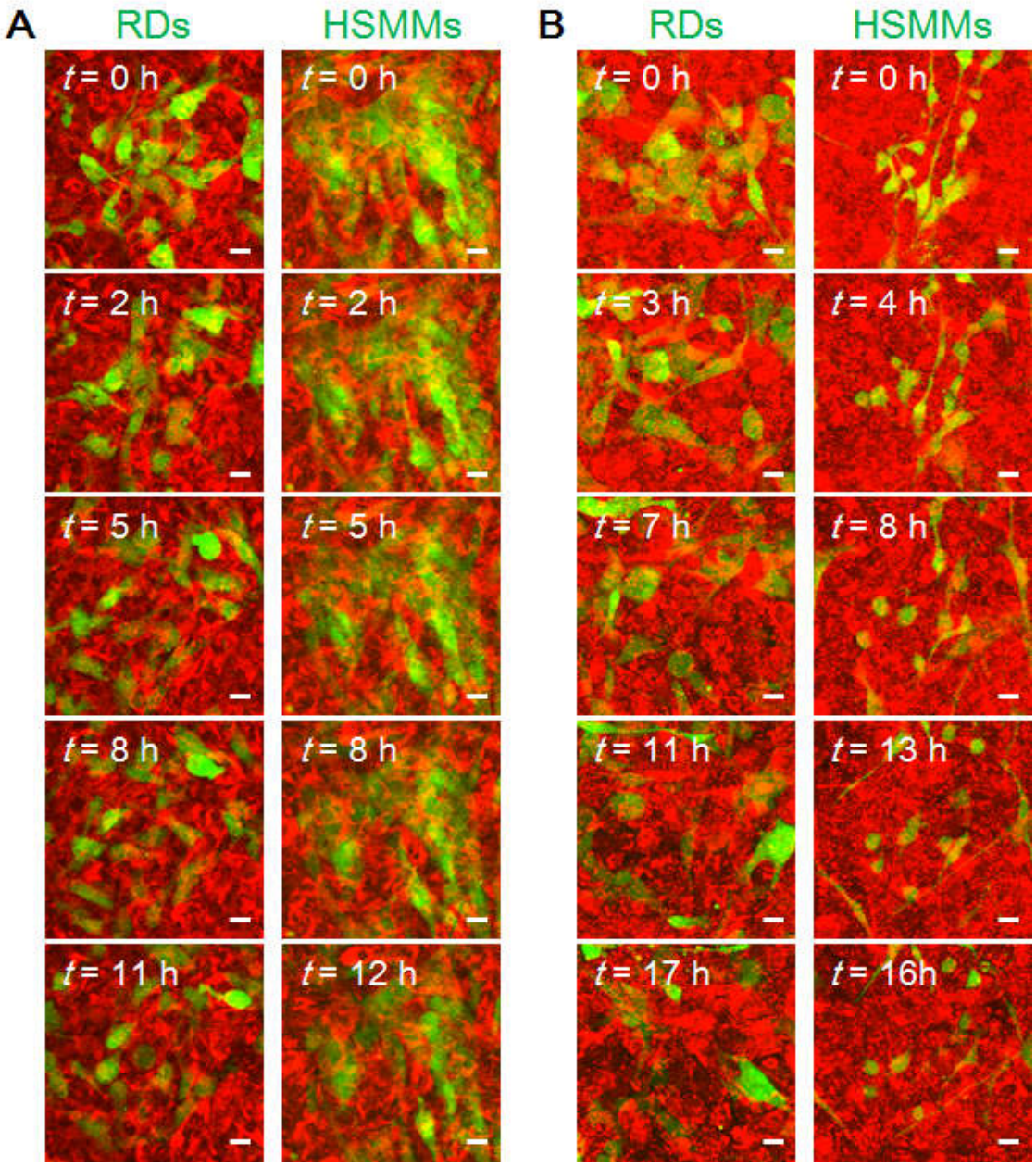

Figure 3-6 Time-lapse observation of target cells in HSMM sheet (**A**) and RD sheet (**B**) at high seeding density. Scale bar: 20 μm.

3.3.4 RD disruption of HSMM alignment and disorder of heterogeneous cell sheet structure

To understand how the HSMM sheet was disrupted by a low ratio of RDs, time-course observation was conducted using confocal laser scanning microscopy with a 60x objective lens. RDs were stained to appear green on captured images to differentiate them from surrounding HSMMs (10% of HSMMs were stained to be green in the control HSMM sheet). At the beginning of culture, RDs distributed homogeneously in the mixed sheet (**Figure 3-7**). In the HSMM control sheet, migration of HSMMs was also random with no alignment observed at $t = 0$. As culture time elapsed, HSMMs gradually aligned with each other in the control sheet, which was an important event in myoblast differentiation. In the HSMM sheet mixed with 10% RDs, HSMM alignment was disrupted and the overall environment of the sheet was chaotic compared with the control HSMM sheet.

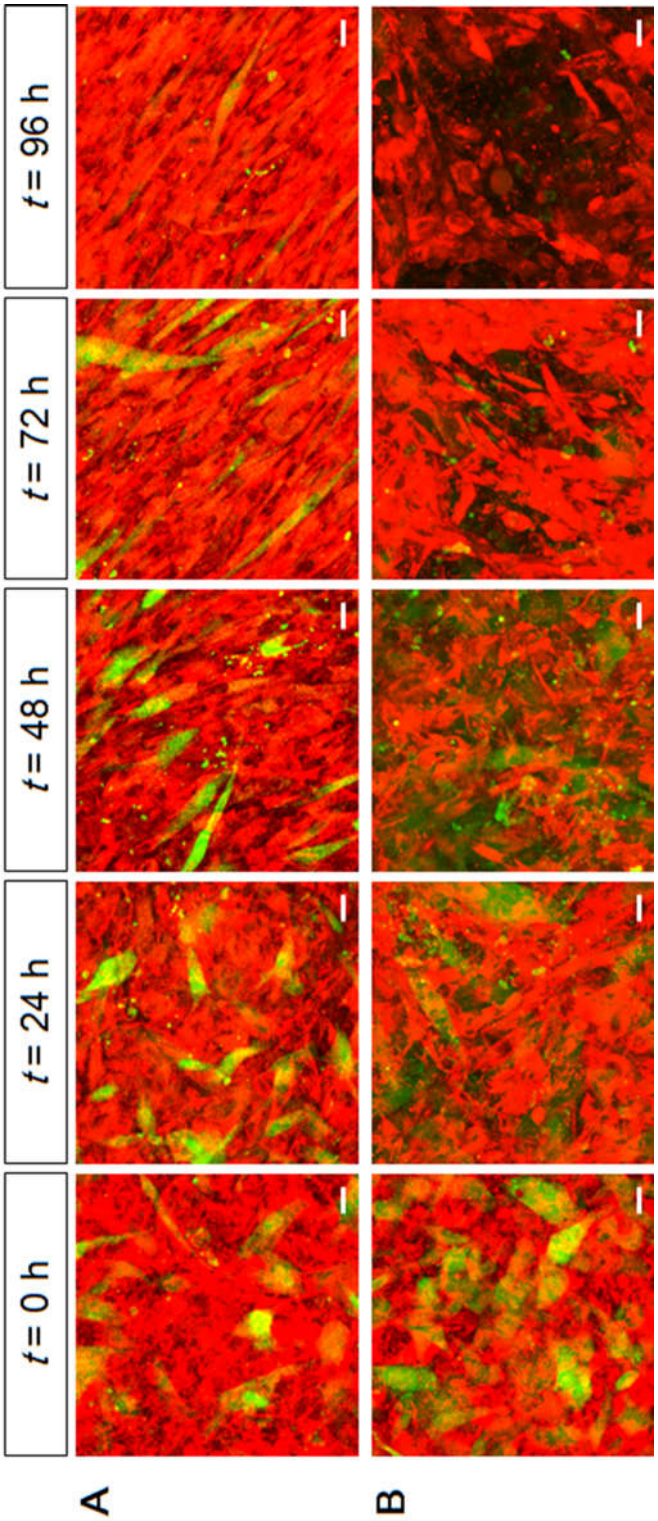

Figure 3-7 Time course of HSMM alignment in multilayered cell sheet. (**A**) Control HSMM sheet, both green and red cells are HSMMs. (**B**) HSMM sheet (red) mixed with 10% of RDs (green). Scale bar: 20 μm.

3.4 Discussion

In this chapter, heterogeneous tumor cell sheets were constructed by co-culturing RDs and HSMMs to investigate heterotypic interactions between a tumor and its host tissue. Disruption of sheet structure was observed in heterogeneous cell sheets with low ratios of RDs (less than 50%); whereas, homogeneous HSMM or RD sheets maintained intact structure (**Figure 3-2**). Deeper exploration of dynamic tumor cell behavior inside HSMM sheets revealed that HSMM alignment was disrupted by highly motile RDs (**Figure 3-7**). This study demonstrated that RMS cells are capable of inducing disorder within their surrounding environment via decay of myoblast alignment.

In our previous studies, an HSMM sheet was proposed for establishing fluidic plate-shaped cell aggregates that provide a 3D platform to understand cell behavior (Kino-oka *et al.*, 2012). Cell sheets differ from other static scaffolds made by isolated or synthetic matrices in that they are capable of generating fluidity from movements of constituent cells. In this chapter, a five-layered tumor cell sheet with constant seeding densities was successfully constructed and characterized by higher fluidity than normal HSMM sheets (**Figure 3-3**). This could be a result of deficient cellular adhesive molecules (Charrasse *et al.*, 2004) and increased migration potential (Meriane *et al.*, 2002; Onisto *et al.*, 2005) of RDs. Although multicellular tumor spheroids have been widely used to resemble *in vivo* tumors, these models frequently experience failure because of their weak connections and inadequate ECM secretion (Ivascu and Kubbies, 2006). This reveals that tumor spheroids are loosely compacted compared with normal cell spheroids. It is reported that large extracellular spaces exist in multicellular spheroids fabricated by rat RMS cells (Davies *et al.*, 2002). In cell sheet system, high fluidity within RD sheets revealed that tumor sheets demonstrated lower compactness than normal sheets. This

indicated that the bulk properties of the sheet were dependent on building cell types and that sheets fabricated by tumor cells were more dynamic compared with their normal counterparts.

Tissue cells are capable of sensing environmental stiffness and determining the migration strategy based on their surrounding environment (Clark and Vignjevic, 2015; Discher *et al.*, 2005; Kumar *et al.*, 2016). Stiffness and topology of the surrounding ECM affect cell migration, resulting in different cell migration patterns and speeds (Charras and Sahai, 2014). Since sheet fluidity has been shown to be quite different between HSMM and RD sheets, we hypothesized that the migration patterns of target cells could be selectively altered based on the structures were of low or high fluidity. **Figure 3-4** indicates that RDs migrate faster than HSMMs in HSMM sheets. Prior to this research, there was limited knowledge regarding how cells migrate over other cells (Charras and Sahai, 2014). Instead of using an integrin-mediated strategy to migrate, cells rely much more on cell surface adhesion molecules, such as cadherins and proteoglycans. One specific role of E-cadherin reported was to generate adhesive forces required for germ cell migration *in vivo* (Cai *et al.*, 2014; Kardash *et al.*, 2010). Abnormal expression and dysfunctional localization of N-cadherin and M-cadherin in the cellular contact sites was found in RMS cells (Charrasse *et al.*, 2004; Soler *et al.*, 1993). Chapter 2 clarified that RDs migrated faster than surrounding HSMMs in a 3D format. Interestingly, when HSMMs were surrounded by rapidly migrating RDs, the HSMMs failed to initiate active migration and later lost pseudopods formation, causing them to float within the RD sheet in a spherical configuration (**Figure 3-5**).This suggested that RDs were capable of changing their surrounding environment, while HSMMs could not.

Tissue cells can not only sense their environment but also remodel their environment

by anchoring to and pulling on their surroundings to migrate. Tumor cells have been documented to be more adaptive and plastic than normal cells, contributing to their invasive and metastatic abilities (Friedl and Wolf, 2010; Wolf *et al.*, 2003). To initiate tumor metastasis, tumor cells initially invade the surrounding normal tissue, and engage in tissue remodeling. To decipher the mechanism used to accomplish this, heterotypic cell interactions have been studied by mixing different ratios of RDs to HSMMs to construct heterogeneous cell sheets. The overall sheet structures were monitored over culture time. Sheet structures were maintained in mono-culture, and disruption was only found in the heterogeneous cell sheet having a relatively low RD ratio (**Figure 3-2**). Deeper exploration by time-course observation demonstrated that HSMM alignment was disordered by fast and random migration of RDs (**Figure 3-7**). Harjanto *et al.* revealed that a prostate cancer cell line can induce matrix remodeling in a 3D collagen system (Harjanto *et al.*, 2011). Apart from the matrix system, this study demonstrated how the structures of *in vitro* tissue-like cell aggregates could be remodeled by tumor cell participation. Similar destructive effects were reported from an induced zebrafish model, in which disorganization of normal muscle architecture was found in the late stage of ERMS development (Ignatius *et al.*, 2012). The disruptive effect of RDs on the alignment of myoblasts was revealed in this study which suggested heterogeneous tumor cell sheets can be utilized to understand heterotypic cell-cell interactions and remodeling of tumor microenvironment.

3.5 Summary

In this chapter, the heterotypic cell-cell interaction was investigated by co-culturing malignant RMS cells with normal myoblasts in a cell sheet system. In 3D cell crowding conditions, tumor cells flexibly adapt to various conditions, acquire increased migratory phenotype, and were capable of compromising the structure of HSMM sheet. Moreover, the disruptive effect of RDs on myoblast sheet structures was initiated by the decay of myoblasts alignment. This study demonstrated that RMS cells were capable of disordering their surrounding environment through induced decay of HSMM alignment. This suggests that muscle disruption could be a significant byproduct of RMS cell invasion into muscle.

Chapter 4 Tumor angiogenesis in the progression of RMS

4.1 Introduction

Tumor angiogenesis, the process of new blood vessel formation induced by a tumor mass, is an important process in tumor malignancy (Folkman, 1971). In the tumor region of RMS, increased angiogenesis can be found (Bid and Houghton, 2011). Over-expression of vascular endothelial growth factors (VEGFs), basic fibroblast growth factors (bFGFs) and interleukin-8 have been detected in serum and urine samples from RMS patients (Pavlakovic *et al.*, 2001), demonstrating an important role of tumor angiogenesis in the disease malignancy. Tumor angiogenesis has already been identified as a therapeutic target for cancer treatment (Hillen and Griffioen, 2007). However, tumor neovascularization is typically disorganized compared with its healthy counterpart, characterized by a defective endothelial monolayer with abnormal sprouts and large intercellular openings (Dudley, 2012). Tumor neovascularization is thought to impair drug delivery to the tumor core and induce radioresistance due to the hypoxic microenvironment, thereby hampering the effectiveness of chemotherapy and radiotherapy.

Disruption of tumor blood vessel formation is a complex process associated with many factors; however, the exact mechanism has not been fully understood. Recently, overexpression of VEGFs by tumor cells has been considered as one cause of tumor vessel abnormality (Nagy *et al.*, 2009). Targeted therapy against VEGF expression has been performed in an attempt to normalize tumor vasculature prior to subsequent chemotherapy or radiotherapy (Goel *et al.*, 2011). Other studies reported decreased endothelial cell networks along with increasing ECM stiffness (Edgar *et al.*, 2014; Ghajar

et al., 2008). However, these studies failed to demonstrate a direct role for tumor cells in the disorganization of the tumor blood vessels. 3D co-culture of tumor cells and endothelial cells has typically been conducted in a spheroid system, with limited success. Timmins *et al.* observed that a 3D branched endothelial network formed when single endothelial cells were seeded onto HCT116 spheroids (Timmins *et al.*, 2004). However, quantitative evaluation of endothelial network formation is difficult in a spheroid aggregate.

Intact cell sheets can be harvested on temperature-responsive PNIPAAm grafted surfaces by lowering the temperature to less than 32ºC (Okano *et al.*, 1995; Sawa and Miyagawa, 2013). Cell sheets preserve both the cells and the naturally formed ECM, thus closely mimicking the true *in vivo* conditions. Using this 3D model, observation of cell behaviors can be divided into the X-Y plane and the Z-axis, enabling temporal and spatial interpretation (Kino-oka *et al.*, 2012). In chapter 2 and 3, we observed active and rapid migration of malignant RDs in the HSMM sheet. Disruption of sheet structure was observed in the heterogeneous cell sheets when co-cultured with 10%–50% tumor cells (**Figure 3-2**). In this chapter, a tumor-containing cell sheet was prepared by mixing a small population of RDs with HSMMs and co-cultured with GFP-HUVECs. The effect of this small population of tumor cells on the behavior of endothelial cells and network formation was investigated.

4.2 Materials & Methods

4.2.1 Cell preparation

Human skeletal muscle myoblasts (HSMMs, Lot. No. 4F1619; Lonza Walkersville Inc.), a human embryonal RMS cell line (RD, Cat. No. EC85111502, American Type Culture Collection) and green fluorescence expressing human umbilical vein endothelial cells (GFP-HUVECs, Lot. No.20100201001, Angio-Proteomie, MA, USA) were used in this study. HSMMs were subcultured on laminin-coated surfaces at 37°C in an atmosphere of 5% CO_2 in Dulbecco's Modified Eagle's Medium (DMEM; Sigma-Aldrich) containing 10% fetal bovine serum (FBS, Thermo Fisher Scientific) and antibiotics (100 U/cm^3 penicillin G, 0.1 mg/cm^3 streptomycin, and 0.25 mg/cm^3 amphotericin B; Invitrogen). RDs were grown in the same medium as the HSMMs without laminin coating. GFP-HUVECs were cultured in a commercially available medium (EGM-2; Lonza Walkersville Inc.). The medium depth was set to 2 mm throughout the experiments. All cells were harvested until 70%–80% confluency.

4.2.2 Incubation of five-layered tumor-containing cell sheet with GFP-HUVECs

RDs and HSMMs harvested from subcultures were stained using a fluorescent reagent (CellTracker^{TM} Orange, Invitrogen), according to the commercial instructions. A monolayer tumor-containing cell sheet was prepared by mixing 8% RDs with HSMMs at a final seeding density of 3.5×10^5 cells/cm^2 then seeded onto the temperature-responsive 24-well Upcell^{TM} plate (CellSeed). The seeded cells were incubated for 24 h at 37^{o}C in a 5% CO_2 atmosphere to form the monolayer sheet. A five-layered tumor-containing cell sheet was constructed and transferred to a 35-mm culture dish (ibidi GmbH) with pre-cultured GFP-HUVECs (Nagamori *et al.*, 2013), as shown in **Figure 4-1**. A five-layered

HSMM sheet without RDs was used as a control sheet. GFP-HUVECs were seeded at a density of 5.0×10^3 cells/cm^2 in EGM-2 medium supplemented with 20% (v/v) FBS and incubated at 37ºC in a 5% CO_2 atmosphere for 24 h. A commercially available medium (SkGM-2; Lonza Walkersville Inc.) supplemented by 10 ng/ml bFGF (ReproCell Inc., NJ, USA) was adapted for co-incubation of the tumor-containing cell sheet with GFP-HUVECs. During the incubation period, the medium was renewed every 24 h. The morphology of GFP-HUVECs was observed using a fluorescence microscope (IN Cell Analyzer 2000, GE Healthcare) with a 10× objective lens every 24 h. Time-lapse observation of the endothelial network formation was conducted by obtaining images every hour at several positions with a 10× objective lens using a confocal laser scanning microscope (FV10i; Olympus).

4.2.3 Evaluation of endothelial network formation inside cell sheet

Evaluation of the endothelial network formation was based on a previously described method (Nagamori *et al.*, 2013) which is shown in **Figure 4-2**. Briefly, the images were captured using a confocal laser scanning microscope (FV10i; Olympus) with a 10× objective lens at more than eight positions in each sample. Each image was 8-bit gray scale with a size of 256×256 pixels and covered an area of 1.27×1.27 mm. Image processing was performed using commercialized software (Image-Pro Plus, Media Cybernetics Inc., MD, USA). The total network length per image area (L; mm^{-1}), and the number of total tips of the network (N_T; tip/mm^2) were measured to calculate the extent of network (L/N_T; mm/tip).

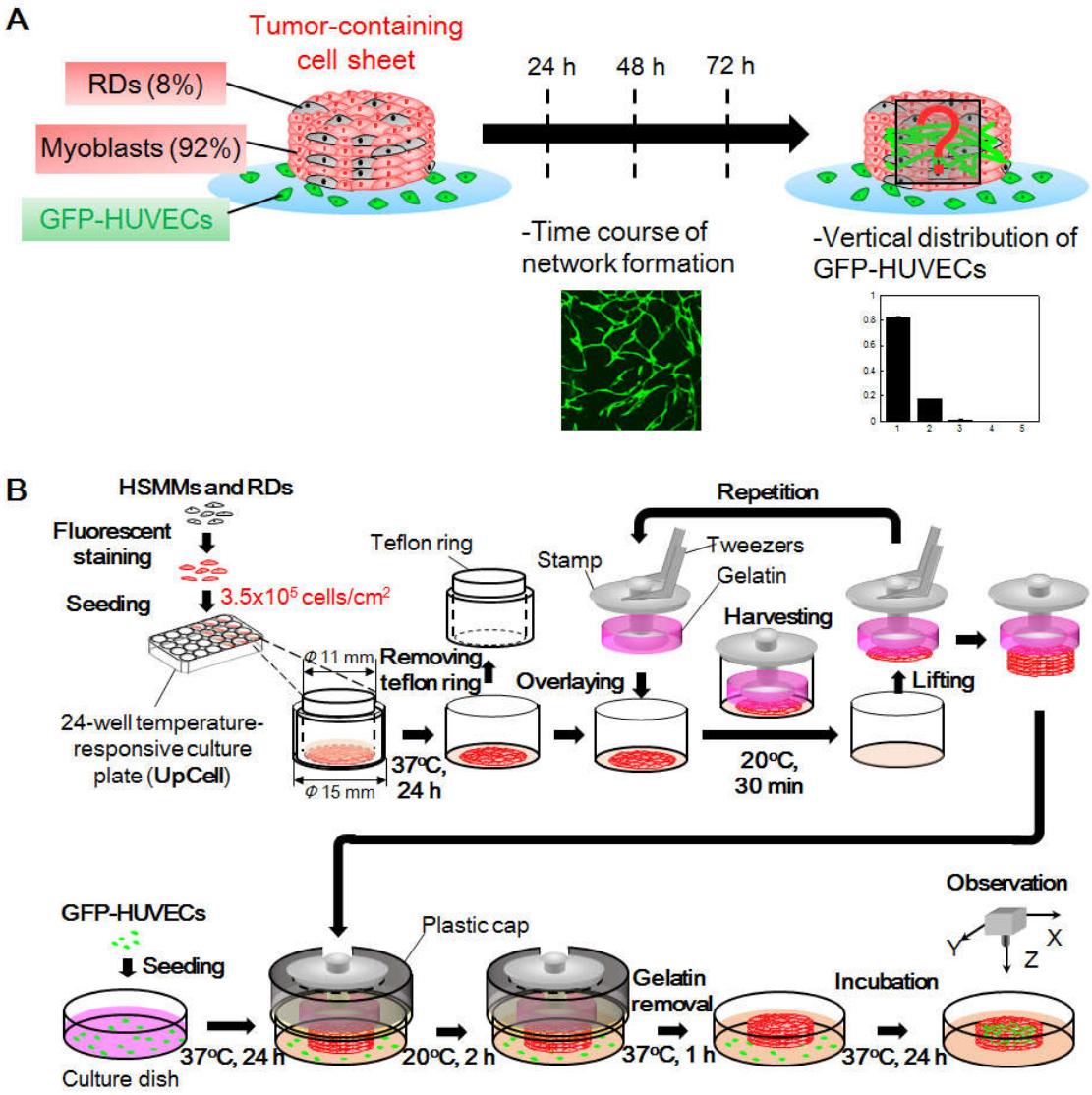

Figure 4-1 Experimental procedure. (A) Schematic drawing. (B) The method of stacking multilayered cell sheets and co-culturing with GFP-HUVECs.

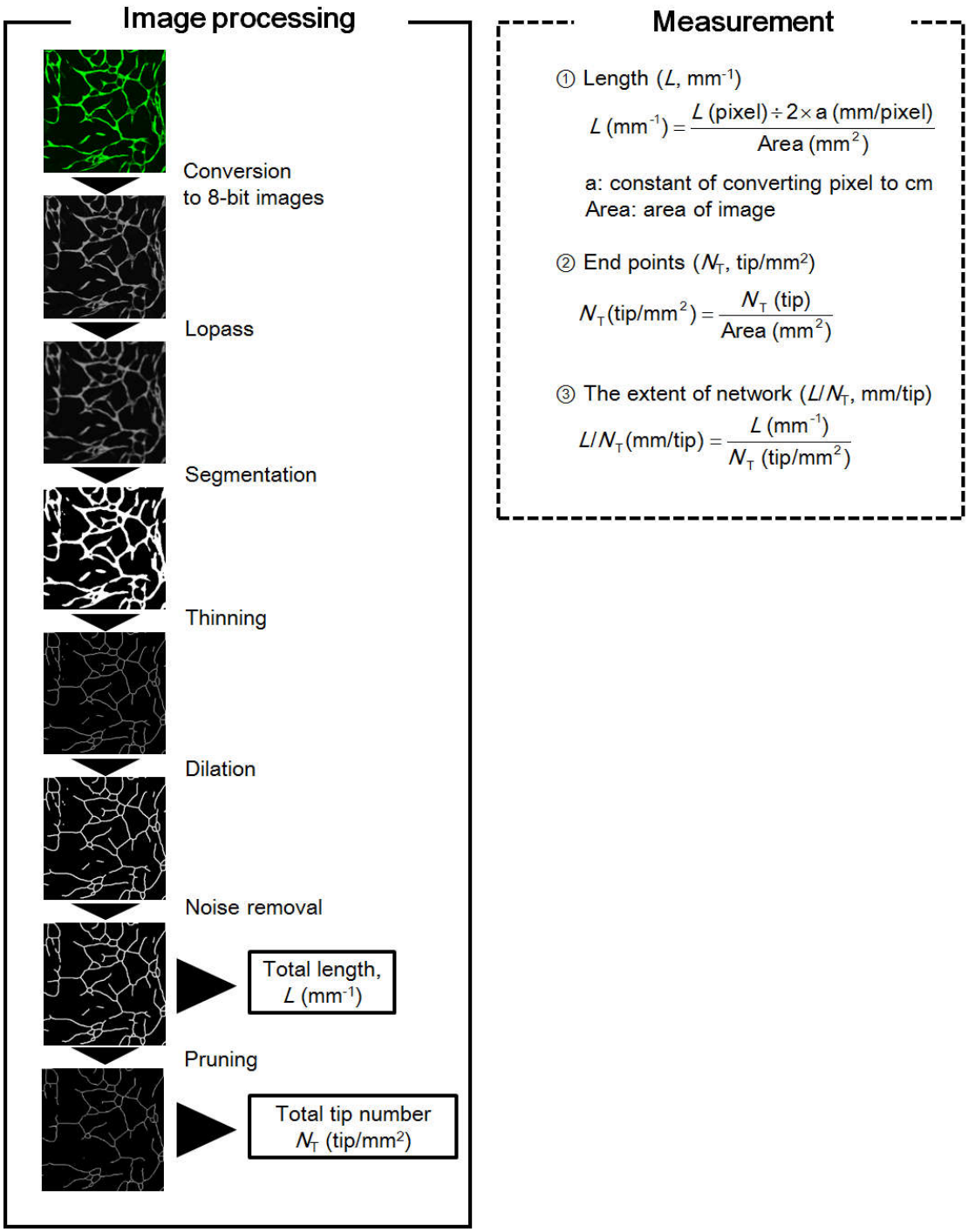

Figure 4-2 Image processing procedure and measurement method to evaluate endothelial network formation.

4.2.4 Immunofluorescence staining of fibronectin in monolayer tumor-containing cell sheet

Fibronectin structure was measured in the monolayer tumor-containing cell sheet. The monolayer tumor-containing cell sheet was cultured in SkGM-2 medium supplemented with 10 ng/ml bFGF for 96 h. The samples were fixed with 4% paraformaldehyde (Wako Pure Chemical Industries) in PBS for 15 min at room temperature and rinsed twice with PBS. The samples were then incubated in PBS containing 0.5% polyoxyethylene octylphenyl ether (Wako Pure Chemical Industries) for 5 min and then blocked in 1% (w/v) bovine serum albumin (BSA; Wako Pure Chemical Industries) in PBS for 90 min at room temperature. The specimens were incubated with primary antibody against human fibronectin (F7387, Sigma-Aldrich) at 4ºC overnight. The samples were rinsed in PBS for three times and reacted with secondary antibodies (Alexa Flour 594-conjugated anti-mouse IgG; Life Technologies) for 1 h at room temperature. Images were captured using a confocal laser scanning microscope (FV1000; Olympus) with a 60× objective lens.

4.2.5 Evaluation of sheet fluidity in tumor-containing cell sheet

Evaluation of sheet fluidity in the tumor-containing cell sheets and control sheet was same as described above. Briefly, a five-layered cell sheet with a basal layer (stained using CellTracker™ Green) and upper layers (stained using CellTracker™ Orange) was prepared for spatial distribution observation using a confocal laser scanning microscope (FV1000; Olympus) with a 60× objective lens at 9 random positions in each sample. Original 8-bit images (256×256 pixels) of both colors in each slice were converted into binary images after identifying intensity threshold values. The ratio of green pixels to the

sum of green pixels in each slice was normalized to determine the distribution of green pixels by dividing into five layers. The normalized distribution of green pixels was assumed to be equivalent to the green cell distribution in the sheet, which was considered to be the frequency of green cells, f_G, in each layer. To quantify sheet fluidity, the diffusivity (D, $\mu m^2/h$) was applied to measure vertical distribution of target cells based on Fick's second law, $\frac{\partial f_G}{\partial t} = D\frac{\partial^2 f_G}{\partial h^2}$, in which f_G, t and h represent the green cell frequency, incubation time, and sheet thickness, respectively. The Crank-Nicolson finite difference method and least squares method were applied to calculate the diffusivity using customized software designed by LabVIEW (National Instruments).

4.2.6 Vertical distribution of GFP-HUVECs in tumor-containing cell sheet

Five-layered tumor-containing cell sheets and control sheets were stained with a fluorescent reagent (CellTracker^{TM} Orange, Invitrogen) and co-cultured with GFP-HUVECs at a seeding density of 2.0 x 10^3 cells/cm^2 for early individual cell migration (at t = 12 h) and 5.0 × 10^3 cells/cm^2 for final localization of GFP-HUVECs with network formation at t = 96 h. Vertical distribution of GFP-HUVECs inside the tumor-containing cell sheets and control sheets was observed by a confocal laser scanning microscope (FV1000; Olympus) with a 60× objective lens. The frequency of green cells (f_G) in each layer was analyzed by using the same method described above.

4.2.6 Transwell experiment

The effect of cytokines secreted from tumor cells on endothelial network formation was investigated by using the polyester membrane transwell-clear inserts with the 0.4 μm pore size (Corning, NY, USA). 2.6 ml of DMEM medium with 10% FBS was firstly

added to the lower chamber. Then 1.5 ml RDs suspension containing the same number as RDs in five-layered tumor-containing cell sheet was added to the upper chamber of the transwell and incubated at 37ºC in a 5% CO_2 atmosphere for 24 h in advance. Five-layered HSMM sheets with or without 8% RDs were constructed as described above and transferred to a 6-well culture plate (Corning) on which GFP-HUVECs were seeded at a density of 5.0×10^3 cells/cm^2. The transwell inserts with RDs were transferred on the top of HSMM sheet and incubated in the SkGM-2 medium supplemented with 10 ng/ml bFGF. The total volume is 4.1 ml according to the commercial instruction. The same volume of medium was added to the co-culture of tumor-containing cell sheet or the control sheet with GFP-HUVECs. The medium was renewed every 24 h. All samples were fixed at t = 96 h for analyzing the final localization of GFP-HUVECs. Vertical distribution of GFP-HUVECs in cell sheets was observed by a confocal laser scanning microscope (FV1000; Olympus) with a 60× objective lens. The frequency of green cells (f_G) in each layer was analyzed by using the same method described above.

4.2.6 Statistical analysis

Data presented in this study were obtained from three independent cultures and expressed as means with standard deviations (SDs). Student's t-test was used to determine the statistical significance of differences among data sets, and values of $P < 0.05$ were considered significant.

4.3 Results

4.3.1 Endothelial network formation inside the tumor-containing cell sheet

Tumor-containing cell sheets were prepared by mixing 8% RDs with HSMMs. The behavior of GFP-HUVECs in the five-layered tumor-containing cell sheet was observed for 96 h to estimate network formation according to the parameters L, N_T, and L/N_T. Endothelial network formation in a five-layered HSMM sheet without RDs was used as a control. The initial density of GFP-HUVECs was $1.60 \pm 0.03 \times 10^4$ cells/cm^2 and $1.56 \pm 0.12 \times 10^4$ cells/cm^2 in the tumor-containing cell sheet and control sheet, respectively. As shown in **Figure 4-3A**, GFP-HUVECs were observed to be single and round-shaped with early elongation in the tumor-containing cell sheet as well as in the control sheet at the beginning of the incubation period. **Figure 4-3B** shows the quantitative analysis of L, N_T, and L/N_T. At t = 24 h, GFP-HUVECs were found to elongate and connect with each other, resulting in an increase in L and decrease in N_T. Less L/N_T was found in the tumor-containing cell sheet compared with the HSMM sheet. After 24 h, GFP-HUVECs elongated with overlapping each other to form a thick network, and L started to decrease correspondingly. At t = 48 h, the value of L/N_T in the tumor-containing cell sheet and HSMM sheet was 0.29 and 0.30 mm/tip, respectively. Degradation of the endothelial network in the tumor-containing cell sheet was observed, and the value of L/N_T decreased to 0.21 mm/tip at t = 96 h, while the value of L/N_T increased to 0.34 mm/tips in HSMM sheet.

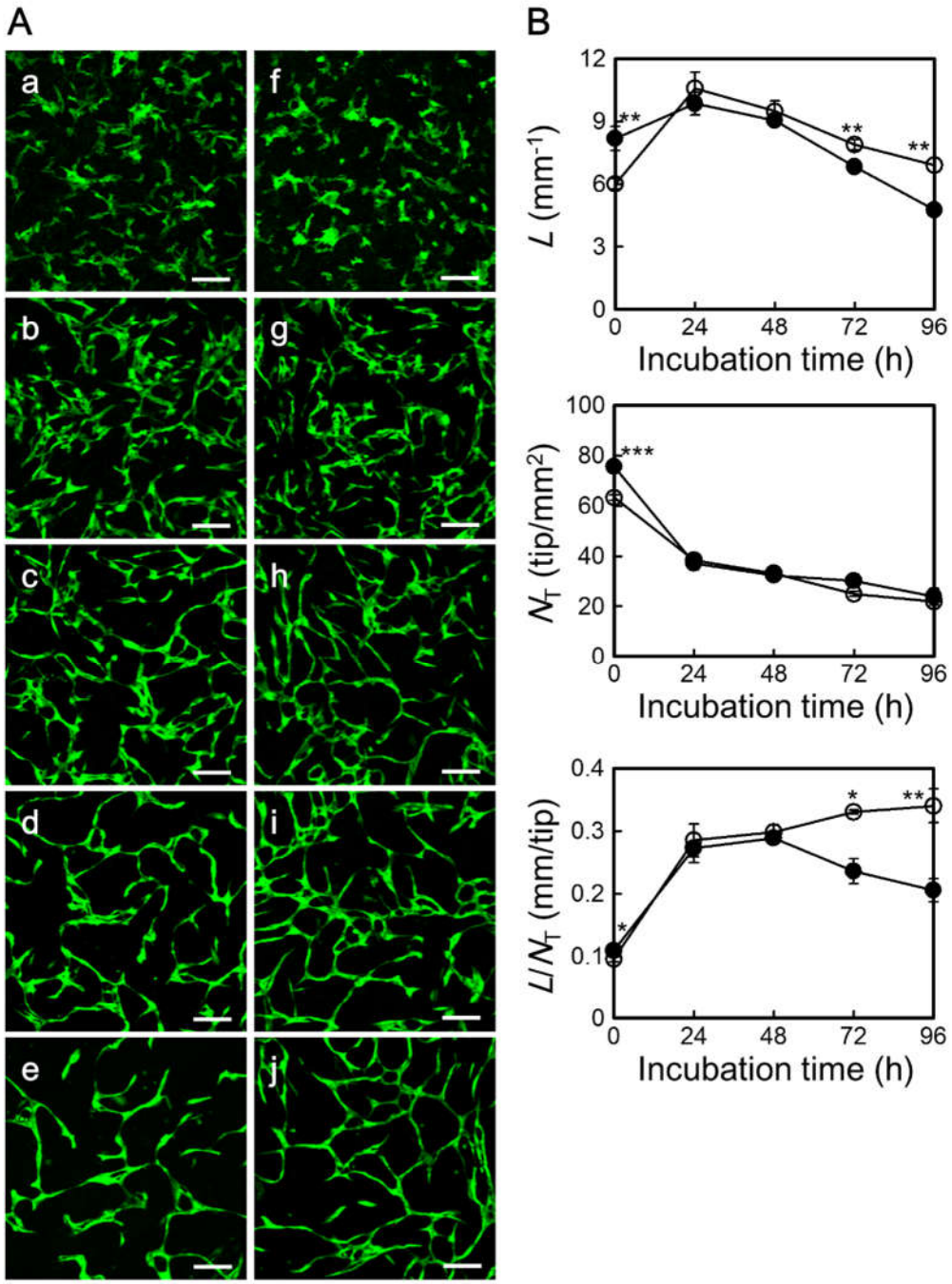

Figure 4-3 Time course of GFP-HUVEC network formation inside the five-layered tumor-containing cell sheet. A: Morphology of GFP-HUVECs in tumor-containing cell sheet (a–e) and control sheet (f–j). Scale bar: 200 μm. B: Quantitative analysis of endothelial network formation. The closed circle and open circle correspond to tumor-containing cell sheet and control sheet, respectively. The bars show the standard deviation (SD) (n = 3). Asterisk indicates significant difference (*: $P < 0.05$; **: $P < 0.01$; ***: $P < 0.001$).

From time-lapse observation, endothelial network was formed by dynamic connections (white arrows) and disconnections (red arrows) among endothelial cells. **Figure 4-4** illustrates the endothelial network at the endpoint in each period. From 24 h to 48 h, the frequency of connection and disconnection is balanced in both cases. From 48 h to 72 h, more red arrows against white arrows was observed in tumor-containing cell sheet, which indicated the degradation of endothelial network. This trend is continuously observed from 72 h to 96 h, resulting in small and branched network.

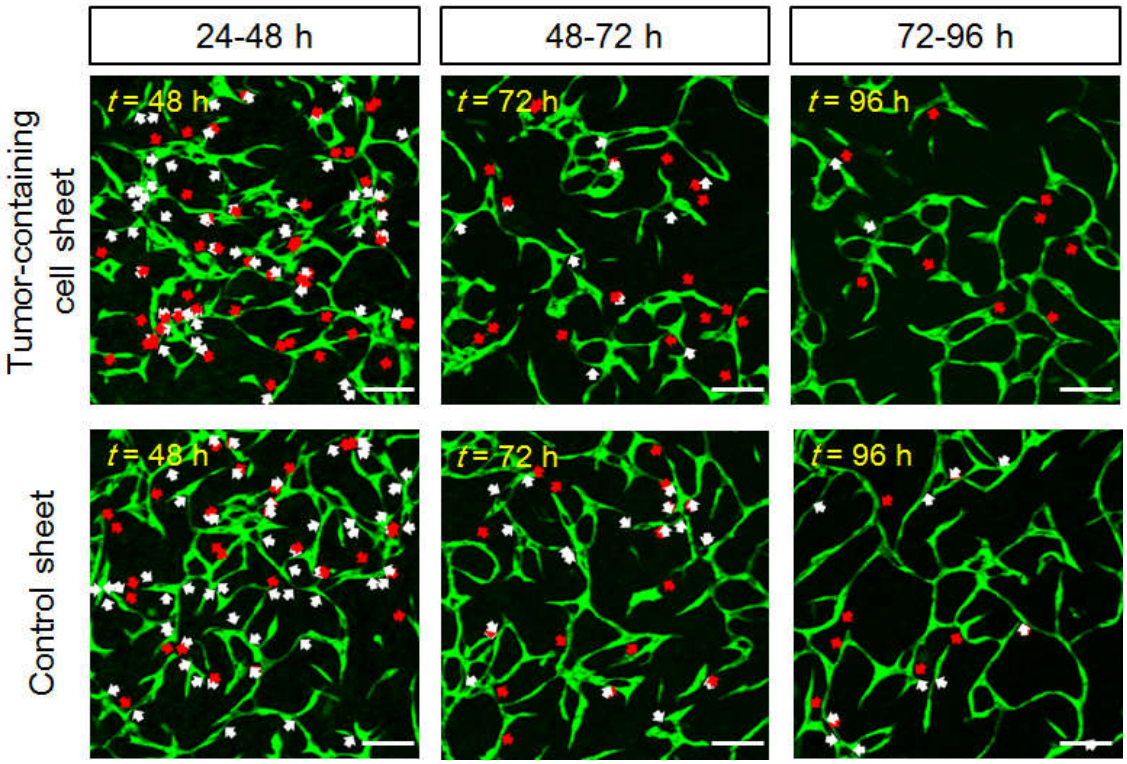

Figure 4-4 Connections (white arrows) and disconnections (red arrows) in endothelial network formation. Scale bar: 200 μm.

4.3.2 Disordered fibronectin meshwork in monolayer tumor-containing cell sheet

Fibronectin assembly was observed by immunofluorescence staining of fibronectin in the monolayer sheet at t = 96 h (**Figure 4-5**). Initially, the fibronectin structure was

discontinuous and disordered in both the tumor-containing and HSMM monolayer. After 96 h of culture, alignment of the fibronectin meshwork was disordered in the tumor-containing cell monolayer. In the HSMM monolayer, a continuous assembly and alignment of fibronectin to fibrils was observed, demonstrating the disruptive effect of tumor cells on the ECM structure of the cell sheet.

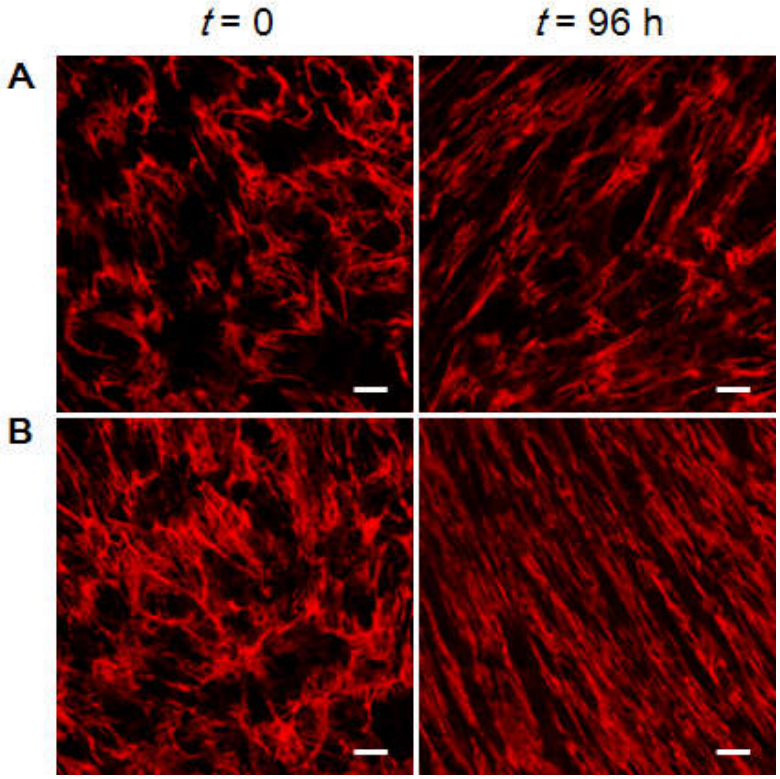

Figure 4-5 Immunofluorescence staining of fibronectin in monolayer of tumor-containing cell sheet (**A**) and control sheet (**B**) at t = 0 and 96 h. Scale bar: 20 μm.

4.3.3 Sheet fluidity increased in tumor-containing cell sheet

Based on the method described previously (Kino-oka *et al.*, 2012), fluidity of the tumor-containing cell sheet was compared with the control sheet. After culturing for 48 h, vertical distribution of the first layer cells was measured to estimate the frequency of green cells (f_G) in each layer. **Figure 4-6A** shows the histogram of f_G in tumor-containing

cell sheet and HSMM sheet. In the tumor-containing cell sheet, the f_G value in the first, second and third layer from the bottom were estimated to be 0.67, 0.29 and 0.03, respectively, while in the HSMM sheet, distribution of 0.77 and 0.21 was calculated in the first and second layer. The vertical diffusivity of green cells, D, in the tumor-containing cell sheet was estimated to be 0.57 μm^2/h, which was 2.7 times higher than that of the HSMM sheet (D = 0.21 μm^2/h), as shown in **Figure 4-6B**.

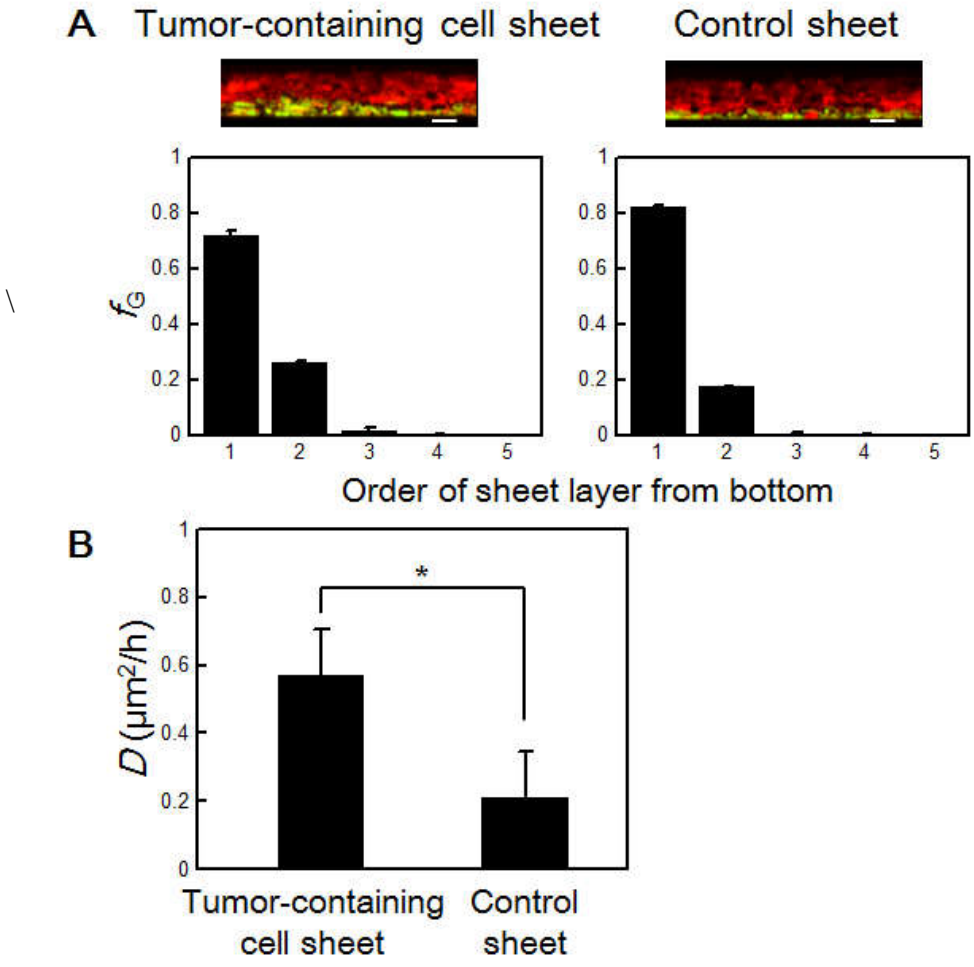

Figure 4-6 Evaluation of sheet fluidity in tumor-containing cell sheet. A: Frequency of the green target cells (f_G) distributed in five layers inside the each sheet at t = 48 h. B: Diffusivity of tumor-containing cell sheet and control sheet. Bars show standard deviation (SD) (n = 3). Asterisk indicates significant difference (*: P < 0.05). Scale bar: 20 μm.

4.3.4 Active migration of endothelia cells in tumor-containing cell sheet

Vertical distribution of GFP-HUVECs was estimated to analyze the migration of these cells. The vertical distribution of GFP-HUVECs at t = 12 h is shown in **Figure 4-7**. In the tumor-containing cell sheet, the frequency of GFP-HUVECs in the first and second layer was estimated to be 0.78 and 0.21, respectively. Most GFP-HUVECs stayed in the first layer in the HSMM sheet, having an f_G value of 0.91. At t = 96 h, most GFP-HUVECs existed in the first and second layer of the control sheet with the f_G value of 0.77 and 0.23 to form the endothelial network. In the tumor-containing cell sheet, 11% of GFP-HUVECs migrated to the fifth layer of the sheet, demonstrating fast migration in the vertical direction.

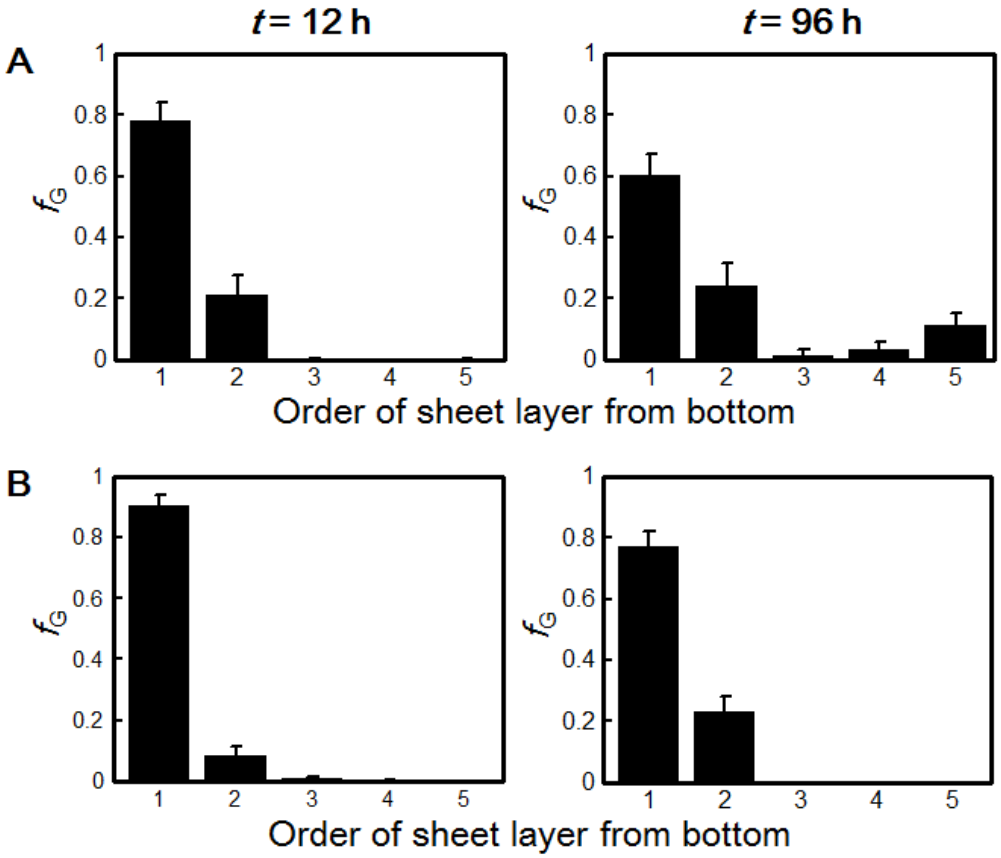

Figure 4-7 Vertical analysis of GFP-HUVEC localization inside the five-layered tumor-containing cell sheet (A) and control sheet (B) at t = 12 h and t = 96 h. Bars show the standard deviation (SD) (n = 3).

4.4 Discussion

Tumor angiogenesis is a prerequisite for initiating tumor malignancy, and blood vessel formation in the tumor region is typically abnormal. In this chapter, a small population of RDs (8%) was found to disrupt the structure of the myoblast sheet, resulting in disordered fibronectin alignment (**Figure 4-5**) and elevated sheet fluidity (**Figure 4-6**). In this highly fluidic sheet, the vertical migration of GFP-HUVECs was increased (**Figure 4-7**) and resulted in the degradation of the endothelial network (**Figure 4-3**) compared with the myoblast sheet without RDs. This observation revealed that small numbers of tumor cells could disrupt the structure of their surrounding microenvironment. The disordered sheet could not support proper endothelial network formation by activation of endothelial cell migration.

In the HSMM sheet, homotypic adhesion, mediated by N-cadherin and M-cadherin, promotes sheet integrity as well as fibronectin alignment, followed by directional cell migration. However, downregulation of N-cadherin and its abnormal function was found in RMS cell lines (Charrasse *et al.*, 2004; Soler *et al.*, 1993), which promotes fast migration of RDs in the HSMM sheet. In chapter 3, RDs were found to migrate rapidly in the HSMM sheet and disrupt normal intercellular adhesions among myoblasts, causing breakdown of myoblast alignment. Individual tumor cells determined the migration strategy depending on the physical properties of their surrounding environment, undergoing mesenchymal or amoeboid migration (Friedl and Wolf, 2003). It was found that RDs migrated in a mesenchymal phenotype with several leading pseudopods in HSMM sheet (**Figure 3-5A**). Tumor cells undergoing mesenchymal migration are dependent on integrin-mediated adhesion and pericellular proteolysis to remodel the structure of normal tissue. ECM meshwork, as well as intercellular adhesions, contributes

to tissue integrity. As assembly of fibronectin into fibrils localizing to the cell surface was required for the accumulation and stability of other ECM proteins (Daley *et al.*, 2008; Sottile and Hocking, 2002), fibronectin meshwork of monolayer sheet was investigated in this study. Our results showed that an ordered fibronectin meshwork generated and arranged by HSMMs was destroyed by the addition of RDs (**Figure 4-5**). RDs are reported to express elevated level of MMPs, such as MMP-2, MMP-9 and MT1-MMP, which are associated with cleavage and remodeling of fibronectin (Ito *et al.*, 2004; Onisto, 2005). To quantify the disruption of the cell sheet by tumor cells, we analyzed sheet fluidity. The fluidity of the HSMM sheet containing only a small amount of RDs was elevated 2.7 times higher than that of the control sheet without RDs. RDs created a disordered environment and affected migration of normal myoblasts. These results indicated that a well-aligned HSMM sheet structure with proper fluidity was disordered by a small number of RDs. The disruption of the whole tissue structure was measured both qualitatively and quantitatively by using cell sheet technology.

Tumor cells break adhesions among normal cells as well as alignment of fibronectin in the cell sheet. As activation of endothelial cell migration from quiescent state was considered as a pre-angiogenesis event, vertical migration of endothelial cells was analyzed in this chapter. As shown in **Figure 4-7**, GFP-HUVECs migrated faster in the vertical direction of the tumor-containing cell sheet. A supplementary transwell experiment was performed to eliminate the paracrine effect from RDs. Promotion of vertical migration was observed when RDs were inserted directly into the cell sheet system (**Figure 4-8A**). It has been reported that during tissue remodeling by tumor cells, cleavage of the ECM components reveals more binding sites, which can be detected and utilized by endothelial cells, thus promoting endothelial cell migration (Stupack and

Cheresh, 2002; Xu *et al.*, 2001). In our system, the fibronectin meshwork was disrupted, potentially exposing ligands, which may support fast migration of endothelial cells.

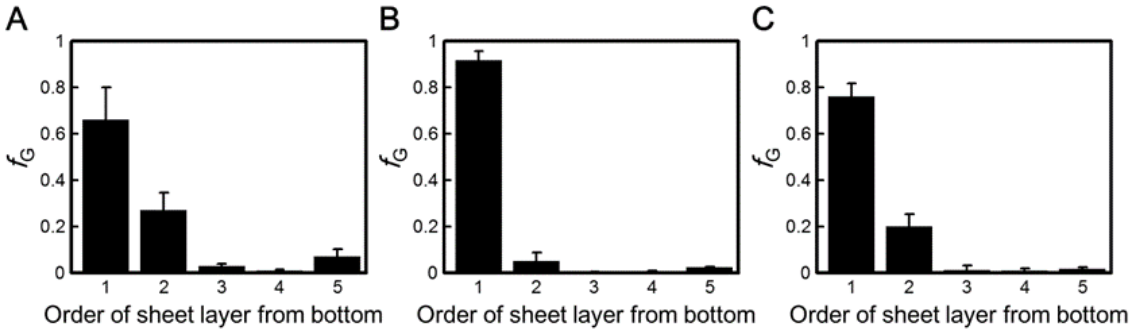

Figure 4-8 Vertical analysis of GFP-HUVEC localization inside the five-layered sheet at t = 96 h. A: Tumor-containing cell sheet. B: RDs pre-cultured on the transwell inserts and co-incubated with HSMM sheet. C: Control sheet. Bars show standard deviation (SD) (n = 3).

Tumor angiogenesis has been identified as an important trigger in tumor malignancy. Traditionally, the effect of tumor cells on angiogenesis was studied in 2D or 3D gel systems cultured in conditioned medium collected from the pre-culture of tumor cells. These systems failed to study the effect of direct contact from tumor cells on the behavior of endothelial cells. Onisto *et al.* reported the expression of VEGFs and MMPs in most RMS cell lines and the promotion of endothelial network formation in the Matrigel system cultured in conditioned medium collected from those cell lines (Onisto, 2005). To the best of our knowledge, the effect of RMS cells on endothelial cell behavior has not been studied in a 3D cell-based system. Our previous work demonstrated that an endothelial network was formed in normal HSMM sheets (Nagamori *et al.*, 2013; Ngo *et al.*, 2013). The addition of a small population of RDs resulted in a high fluidic sheet and the endothelial cells adapted to this disordered structure with a fast migratory phenotype. As

endothelial network formation is a dynamic process with alternating connections and disconnections, fast migration of HUVECs increased the frequency of disconnection (**Figure 4-4**). Although an endothelial network was initially established (at t = 48 h) in the tumor-containing cell sheet, degradation of the network was observed at the end of culture. By disrupting the sheet structure, RDs altered the behavior of endothelial cells, thus causing abnormalities in the endothelial network formation, which suggested the facilitation of tumor angiogenesis.

4.5 Summary

In this chapter, the effect of minor tumor cells on endothelial cell behavior was investigated by co-culturing tumor-containing cell sheets with endothelial cells. Tumor-containing cell sheets with a disrupted ECM structure and elevated sheet fluidity promoted migration of endothelial cells and increased the frequency of endothelial disconnection. Early degradation of the endothelial network was observed in the tumor-containing cell sheet.

Chapter 5 Concluding remarks

5.1 Summary

RMS is a highly metastatic tumor with low survival ratio. As RMS is always diagnosed with secondary metastasis, the problem is failure to acquire adequate information of primary tumor site. It remains largely unknown the structure of tumor microenvironment at the primary site and the tumor progression of this malignancy. This study focused on the study of embryonal rhabdomyosarcoma progression in a 3D multicellular system constructed by cell sheet technology. As tumor progression is a complex multi-step process, this study is divided into three main parts: 1. Behavior of tumor cell migration in 3D tissue structure; 2. Heterotypic cellular interaction between tumor cells and host tissue cells in tumor invasion; 3. Angiogenesis process influenced by tumor cells.

Firstly, migration ability of human embryonal RMS cells was studied in the 3D HSMM sheet. The analysis of cell migration was divided into vertical migration and horizontal migration to understand migration in a 3D format. Vertical migration of RDs was quantified according to the distribution of RDs in each layer from the bottom to top. It was found that more RDs located towards the upper layer of cell sheet, demonstrating that RDs migrate faster in vertical direction compared with myoblasts. Horizontal migration of target cells was tracked by time-lapse observation and migration rate of RDs was calculated to be 7.35 μm/h, which was 1.5 times faster than that of myoblasts (5.07 μm/h). RDs demonstrated a fast migratory phenotype compared with surrounding myoblasts both in vertical and horizontal direction.

After acquiring high motility, tumor cells will invade into their surrounding

environment to seek a way out. The heterotypic interaction between tumor cells and host tissue cells plays a vital role in this process. In chapter 3, the heterotypic cell-cell interaction was investigated by co-culturing malignant RMS cells with normal myoblasts in a cell sheet. Heterogeneous cell sheet was prepared by mixing different ratios of RDs with HSMMs. The deformation of sheet structure was only observed when RDs were co-cultured with myoblasts at a low ratio; whereas, homogeneous HSMM or RD sheets maintained the intact structure. Further exploration revealed that tumor cells can adapt to their surrounding environment, keep a highly motile feature and remodel the environment, while myoblasts lose migration ability when facing a comparably dynamic environment. A small population of RDs (10%) were capable to disorder the alignment of myoblasts in the cell sheet and finally disrupt the structure of whole cell sheet. It indicated that minor tumor cells can affect the bulk tissue and suggested that muscle disruption could be initiated by RMS invasion.

Tumor angiogenesis is an important trigger of metastasis by providing oxygen and nutrients to the starving primary tumor. In chapter 4, a tumor-containing cell sheet was prepared by mixing RDs with HSMMs at a ratio of 8% to avoid deformation of sheet structure and co-cultured with GFP-HUVECs to understand the effect of tumor cells on endothelial behaviors. The structure of tumor-containing cell sheet differed from the HSMM sheet without tumor cells in disordered fibronectin alignment and elevated sheet fluidity. Interestingly, in highly fluidic tumor-containing cell sheet, the vertical migration of GFP-HUVECs was promoted, finally resulting in the degradation of endothelial network formation. Unlike the conventional study of tumor angiogenesis, which focusing on the cytokines secreted from tumor cells, this chapter studied how the environment change caused by minor RDs affected endothelial network formation. It indicated that

disorganized tissue structure facilitated tumor angiogenesis by activation of endothelial cell migration.

In conclusion, the three important steps of RMS progression were studied in this research. The direct role of tumor cells in tissue remodeling and subsequent influence on angiogenesis was studied, bringing new insights into the field. This study firstly applied cell sheet technology in the *in vitro* study of cancer, revealing the advantages of this technology in the field. In future, drug screening system will be developed based on cell sheet technology and more cancer types will be tested using this method.

5.2 Future perspectives

To continue the research initiated by this work, the following proposals are recommended.

1) Explore more in the mechanism of cell migration using multicellular cell sheet

Phenotypically, tumor cell migration was compared with normal cells and a fast migratory phenotype of tumor cells was confirmed. Cell morphology and migration was observed by time-lapse observation. However, to deeply explore the mechanism of cell migration facing 3D environment, there is a limitation of cell sheet system. Due to the multicellular feature of cell sheet, it is difficult to investigate the gene expression of the component cells using endpoint analysis. Therefore, transgenic manipulation of target cells in advance, such as downregulation or upregulation of genes related to migration (e.g. N-cadherin) or introducing fluorescence-labeled proteins into target cells, will be helpful to elucidate the mechanism during tumor cell migration.

2) Apply to other cancer types

Rhabdomyosarcoma is the first *in vitro* cancer model constructed by cell sheet engineering. However, every cancer is specific to its origins, development process and treatment. In future, more cancers can be modeled using cell sheet technology.

3) Apply for drug screening

3D cell culture has been highlighted as a prospective system for drug screening, filling the gap between *in vitro* 2D culture and animal test. This work initially studied the tumor cell behaviors and proposed to model the phenomenon occurred during embryonal rhabdomyosarcoma progression, such as invasion and angiogenesis. More efforts need to make in future to apply these models for cancer drug screening.

Nomenclature

f_G	Frequency of green target cells in each layer of the cell sheet	[-]
h	Thickness of the cell sheet	[μm]
t	Incubation time	[h]
D	Diffusivity of target cells	[μm^2/h]
(x_i, y_i)	The centroids of each cell	
d_i	Cell displacement during each time interval	μm
V	Horizontal migration rate of target cells	[μm/h]
L	Total length of endothelial network formation	[mm^{-1}]
N_T	Total tip number of endothelial network formation	[tip/mm^2]
L/N_T	The extent of endothelial network formation	[mm/tip]

References

Akimoto, J., Takagi, S., Nakayama, M., Arauchi, A., Yamato, M., and Okano, T. (2013). Transplantation of cancerous cell sheets effectively generates tumour-bearing model mice. J. Tissue Eng. Regen. Med. DOI: 10.1002/term.1850.

Anderson, J., Gordon, A., Pritchard-Jones, K., and Shipley, J. (1999). Genes, chromosomes, and rhabdomyosarcoma. Genes Chromosomes Cancer *26*, 275-285.

Avirneni-Vadlamudi, U., Galindo, K.A., Endicott, T.R., Paulson, V., Cameron, S., and Galindo, R.L. (2012). Drosophila and mammalian models uncover a role for the myoblast fusion gene TANC1 in rhabdomyosarcoma. J. Clin Invest *122*, 403-407.

Bach, T.L., Barsigian, C., Chalupowicz, D.G., Busler, D., Yaen, C.H., Grant, D.S., and Martinez, J. (1998). VE-Cadherin Mediates Endothelial Cell Capillary Tube Formation in Fibrin and Collagen Gels. Exp. Cell Res. *238*, 324-334.

Baumann, K. (2012). Cell migration: Switching to 3D. Nat. Rev. Mol. Cell Biol. *13*, 338-339.

Belyea, B., Kephart, J.G., Blum, J., Kirsch, D.G., and Linardic, C.M. (2012). Embryonic signaling pathways and rhabdomyosarcoma: contributions to cancer development and opportunities for therapeutic targeting. Sarcoma *2012*, 406239.

Bid, H.K., and Houghton, P.J. (2011). Targeting angiogenesis in childhood sarcomas. Sarcoma *2011*, 601514.

Bogdanowicz, D.R., and Lu, H.H. (2013). Studying cell-cell communication in co-culture. Biotechnol. J. *8*, 395-396.

Breier, G. (2000). Angiogenesis in Embryonic Development-A Review. Placenta *21, Supplement A*, S11-S15.

Cai, D., Chen, S.C., Prasad, M., He, L., Wang, X., Choesmel-Cadamuro, V., Sawyer, J.K.,

Danuser, G., and Montell, D.J. (2014). Mechanical feedback through E-cadherin promotes direction sensing during collective cell migration. Cell *157*, 1146-1159.

Chandrasekaran, S., Geng, Y., DeLouise, L.A., and King, M.R. (2012). Effect of homotypic and heterotypic interaction in 3D on the E-selectin mediated adhesive properties of breast cancer cell lines. Biomaterials *33*, 9037-9048.

Charras, G., and Sahai, E. (2014). Physical influences of the extracellular environment on cell migration. Nat. Rev. Mol. Cell Biol. *15*, 813-824.

Charrasse, S., Comunale, F., Gilbert, E., Delattre, O., and Gauthier-Rouviere, C. (2004). Variation in cadherins and catenins expression is linked to both proliferation and transformation of rhabdomyosarcoma. Oncogene *23*, 2420-2430.

Chung, A.S., and Ferrara, N. (2011). Developmental and pathological angiogenesis. Annu. Rev. Cell Dev. Biol *27*, 563-584.

Clark, A.G., and Vignjevic, D.M. (2015). Modes of cancer cell invasion and the role of the microenvironment. Curr. Opin. Cell Biol. *36*, 13-22.

Condeelis, J., and Segall, J.E. (2003). Intravital imaging of cell movement in tumours. Nat. Rev. Cancer *3*, 921-930.

Daley, W.P., Peters, S.B., and Larsen, M. (2008). Extracellular matrix dynamics in development and regenerative medicine. J. Cell Sci. *121*, 255-264.

Dantonello, T.M., Winkler, P., Boelling, T., Friedel, G., Schmid, I., Mattke, A.C., Ljungman, G., Bielack, S.S., Klingebiel, T., Koscielniak, E. (2011). Embryonal rhabdomyosarcoma with metastases confined to the lungs: report from the CWS Study Group. Pediatr. Blood Cancer *56*, 725-732.

Davies, C.d.L., Berk, D.A., Pluen, A., and Jain, R.K. (2002). Comparison of IgG diffusion and extracellular matrix composition in rhabdomyosarcomas grown in mice versus

in vitro as spheroids reveals the role of host stromal cells. Br. J. Cancer *86*, 1639-1644.

Discher, D.E., Janmey, P., and Wang, Y. L. (2005). Tissue Cells Feel and Respond to the Stiffness of Their Substrate. Science *310*, 1139-1143.

Dudley, A.C. (2012). Tumor endothelial cells. Cold Spring Harb. Perspect. Med. *2*, a006536.

Duguay, D., Foty, R.A., and Steinberg, M.S. (2003). Cadherin-mediated cell adhesion and tissue segregation: qualitative and quantitative determinants. Dev. Biol. *253*, 309-323.

Edgar, L.T., Underwood, C.J., Guilkey, J.E., Hoying, J.B., and Weiss, J.A. (2014). Extracellular matrix density regulates the rate of neovessel growth and branching in sprouting angiogenesis. PloS one *9*, e85178.

Edmondson, R., Broglie, J.J., Adcock, A.F., and Yang, L. (2014). Three-dimensional cell culture systems and their applications in drug discovery and cell-based biosensors. *12*, 207-218.

Fleischmann, A., Jochum, W., Eferl, R., Witowsky, J., and Wagner, E.F. (2003). Rhabdomyosarcoma development in mice lacking Trp53 and Fos: Tumor suppression by the Fos protooncogene. Cancer Cell *4*, 477-482.

Folkman, J. (1971). Tumor Angiogenesis: Therapeutic Implications. N. Eng. J. Med. *285*, 1182-1186.

Folkman, J. (2006). Angiogenesis. Annu. Rev. Med. *57*, 1-18.

Friedl, P., and Alexander, S. (2011). Cancer invasion and the microenvironment: plasticity and reciprocity. Cell *147*, 992-1009.

Friedl, P., Sahai, E., Weiss, S., and Yamada, K.M. (2012). New dimensions in cell

migration. Nat. Rev. Mol. Cell Biol. *13*, 743-747.

Friedl, P., and Wolf, K. (2003). Tumour-cell invasion and migration: diversity and escape mechanisms. Nat. Rev. Cancer *3*, 362-374.

Friedl, P., and Wolf, K. (2010). Plasticity of cell migration: a multiscale tuning model. J. Cell Biol. *188*, 11-19.

Friedl, P., Zanker, K.S., and Brocker, E.B. (1998). Cell migration strategies in 3-D extracellular matrix: differences in morphology, cell matrix interactions, and integrin function. Microsc. Res. Tech. *43*, 369-378.

Galindo, R.L., Allport, J.A., and Olson, E.N. (2006). A Drosophila model of the rhabdomyosarcoma initiator PAX7-FKHR. Proc. Natl. Acad. Sci. U.S.A. *103*, 13439-13444.

Ghajar, C.M., Chen, X., Harris, J.W., Suresh, V., Hughes, C.C.W., Jeon, N.L., Putnam, A.J., and George, S.C. (2008). The effect of matrix density on the regulation of 3-D capillary morphogenesis. Biophys. J. *94*, 1930-1941.

Goel, S., Duda, D.G., Xu, L., Munn, L.L., Boucher, Y., Fukumura, D., and Jain, R.K. (2011). Normalization of the vasculature for treatment of cancer and other diseases. Physiol. Rev. *91*, 1071-1121.

Haraguchi, Y., Shimizu, T., Sasagawa, T., Sekine, H., Sakaguchi, K., Kikuchi, T., Sekine, W., Sekiya, S., Yamato, M., Umezu, M., and Okano, T. (2012). Fabrication of functional three-dimensional tissues by stacking cell sheets in vitro. Nat. Protoc. *7*, 850-858.

Harjanto, D., Maffei, J.S., and Zaman, M.H. (2011). Quantitative analysis of the effect of cancer invasiveness and collagen concentration on 3D matrix remodeling. PloS one *6*, e24891.

Hettmer, S., and Wagers, A.J. (2010). Muscling in: Uncovering the origins of rhabdomyosarcoma. Nat. Med. *16*, 171-173.

Hillen, F., and Griffioen, A.W. (2007). Tumour vascularization: sprouting angiogenesis and beyond. Cancer Metastasis Rev. *26*, 489-502.

Hinson, A.R.P., Jones, R., Crose, L.E.S., Belyea, B.C., Barr, F.G., and Linardic, C.M. (2013). Human rhabdomyosarcoma cell lines for rhabdomyosarcoma research: utility and pitfalls. Front. Oncol. *3*, 183.

Ignatius, M.S., Chen, E., Elpek, N.M., Fuller, A.Z., Tenente, I.M., Clagg, R., Liu, S., Blackburn, J.S., Linardic, C.M., Rosenberg, A.E., Nielsen, P.G., Mempel, T.R., and Langenau, D.M. (2012). In vivo imaging of tumor-propagating cells, regional tumor heterogeneity, and dynamic cell movements in embryonal rhabdomyosarcoma. Cancer Cell *21*, 680-693.

Ito, H., Duxbury, M., Benoit, E., Farivar, R.S., Gardner-Thorpe, J., Zinner, M.J., Ashley, S.W., and Whang, E.E. (2004). Fibronectin-induced COX-2 mediates MMP-2 expression and invasiveness of rhabdomyosarcoma. Biochem. Biophys Res. Commun. *318*, 594-600.

Ivascu, A., and Kubbies, M. (2006). Rapid generation of single-tumor spheroids for high-throughput cell function and toxicity analysis. J. Biomol. Screen. *11*, 922-932.

Ivers, L.P., Cummings, B., Owolabi, F., Welzel, K., Klinger, R., Saitoh, S., O'Connor, D., Fujita, Y., Scholz, D., and Itasaki, N. (2014). Dynamic and influential interaction of cancer cells with normal epithelial cells in 3D culture. Cancer Cell Int. *14*, 108.

Jain, R.K., Munn, L.L., and Fukumura, D. (2002). Dissecting tumour pathophysiology using intravital microscopy. Nat. Rev. Cancer *2*, 266-276.

Kardash, E., Reichman-Fried, M., Maitre, J.L., Boldajipour, B., Papusheva, E.,

Messerschmidt, E.M., Heisenberg, C.P., and Raz, E. (2010). A role for Rho GTPases and cell-cell adhesion in single-cell motility in vivo. Nat. cell Biol. *12*, 47-53.

Kashi, V.P., Hatley, M.E., and Galindo, R.L. (2015). Probing for a deeper understanding of rhabdomyosarcoma: insights from complementary model systems. Nat. Rev. Cancer *15*, 426-439.

Kaufmann, U., Kirsch, J., Irintchev, A., Wernig, A., and Starzinski-Powitz, A. (1999). The M-cadherin catenin complex interacts with microtubules in skeletal muscle cells: implications for the fusion of myoblasts. J. Cell Sci. *112*, 55-67.

Keller, C., Arenkiel, B.R., Coffin, C.M., El-Bardeesy, N., DePinho, R.A., and Capecchi, M.R. (2004). Alveolar rhabdomyosarcomas in conditional Pax3:Fkhr mice: cooperativity of Ink4a/ARF and Trp53 loss of function. Genes Dev. *18*, 2614-2626.

Kino-oka, M., Agatahama, Y., Hata, N., and Taya, M. (2004). Evaluation of growth potential of human epithelial cells by motion analysis of pairwise rotation under glucose-limited condition. Biochem. Eng. J. *19*, 109-117.

Kino-oka, M., Ngo, T.X., Nagamori, E., Takezawa, Y., Miyake, Y., Sawa, Y., Saito, A., Shimizu, T., Okano, T., and Taya, M. (2012). Evaluation of vertical cell fluidity in a multilayered sheet of skeletal myoblasts. J. Biosci. Bioeng. *113*, 128-131.

Kiran, M.S., Viji, R.I., Kumar, S.V., Prabhakaran, A.A., and Sudhakaran, P.R. (2011). Changes in expression of VE-cadherin and MMPs in endothelial cells: implications for angiogenesis. Vascular cell *3*, 6.

Krakhmal, N.V., Zavyalova, M.V., Denisov, E.V., Vtorushin, S.V., and Perelmuter, V.M. (2015). Cancer invasion: patterns and mechanisms. Acta Naturae *7*, 17-28.

Kumar, S., Kapoor, A., Desai, S., Inamdar, M.M., and Sen, S. (2016). Proteolytic and non-proteolytic regulation of collective cell invasion: tuning by ECM density and

organization. Sci. Rep. *6*, 19905.

Langenau, D.M., Keefe, M.D., Storer, N.Y., Guyon, J.R., Kutok, J.L., Le, X., Goessling, W., Neuberg, D.S., Kunkel, L.M., and Zon, L.I. (2007). Effects of RAS on the genesis of embryonal rhabdomyosarcoma. Genes Dev. *21*, 1382-1395.

Langenau, D.M., Keefe, M.D., Storer, N.Y., Jette, C.A., Smith, A.C., Ceol, C.J., Bourque, C., Look, A.T., and Zon, L.I. (2008). Co-injection strategies to modify radiation sensitivity and tumor initiation in transgenic Zebrafish. Oncogene *27*, 4242-4248.

Linardic, C.M., Downie, D.L., Qualman, S., Bentley, R.C., and Counter, C.M. (2005). Genetic modeling of human rhabdomyosarcoma. Cancer Res. *65*, 4490-4495.

Masia, A., Almazan-Moga, A., Velasco, P., Reventos, J., Toran, N., Sanchez de Toledo, J., Roma, J., and Gallego, S. (2012). Notch-mediated induction of N-cadherin and α9-integrin confers higher invasive phenotype on rhabdomyosarcoma cells. Br. J. Cancer *107*, 1374-1383.

Matsuda, N., Shimizu, T., Yamato, M., and Okano, T. (2007). Tissue engineering based on cell sheet technology. Adv. Mater. *19*, 3089-3099.

Matsuyoshi, N., and Imamura, S. (1997). Multiple cadherins are expressed in human fibroblasts. Biochem. Biophys. Res. Commun. *235*, 355-358.

Meriane, M., Charrasse, S., Comunale, F., Mery, A., Fort, P., Roux, P., and Gauthier-Rouviere, C. (2002). Participation of small GTPases Rac1 and Cdc42Hs in myoblast transformation. Oncogene *21*, 2901-2907.

Merlino, G., and Helman, L.J. (1999). Rhabdomyosarcoma - working out the pathways. Oncogene *18*, 5340-5348.

Nagamori, E., Ngo, T.X., Takezawa, Y., Saito, A., Sawa, Y., Shimizu, T., Okano, T., Taya, M., and Kino-oka, M. (2013). Network formation through active migration of human

vascular endothelial cells in a multilayered skeletal myoblast sheet. Biomaterials *34*, 662-668.

Nagamori, E., Oda, M., Nakamura, T., Shimizu, T., Okano, T., and Kino-oka, M. (2014). Spatial habitation of heterogeneous cell population in a multi-Layered myoblast sheet due to the differences in their behaviors of migration and cell-cell connection. Curr. Nanosci. *10*, 173-178.

Nagy, J.A., Chang, S.H., Dvorak, A.M., and Dvorak, H.F. (2009). Why are tumour blood vessels abnormal and why is it important to know? Br. J. Cancer *100*, 865-869.

Nanni, P., Nicoletti, G., De Giovanni, C., Croci, S., Astolfi, A., Landuzzi, L., Di Carlo, E., Iezzi, M., Musiani, P., and Lollini, P.L. (2003). Development of rhabdomyosarcoma in HER-2/neu transgenic p53 mutant mice. Cancer Res. *63*, 2728-2732.

Ngo, T.X., Nagamori, E., Kikuchi, T., Shimizu, T., Okano, T., Taya, M., and Kino-oka, M. (2013). Endothelial cell behavior inside myoblast sheets with different thickness. Biotechnol. Lett. *35*, 1001-1008.

Nishida, K., Yamato, M., Hayashida, Y., Watanabe, K., Yamamoto, K., Adachi, E., Nagai, S., Kikuchi, A., Maeda, N., Watanabe, H.*, et al.* (2004). Corneal reconstruction with tissue-engineered cell sheets composed of autologous oral mucosal epithelium. N. Engl. J. Med. *351*, 1187-1196.

Nishijo, K., Chen, Q.R., Zhang, L., McCleish, A.T., Rodriguez, A., Cho, M.J., Prajapati, S.I., Gelfond, J.A.L., Chisholm, G.B., Michalek, J.E.*, et al.* (2009). Credentialing a preclinical mouse model of alveolar rhabdomyosarcoma. Cancer Res. *69*, 2902-2911.

Oberlin, O., Rey, A., Lyden, E., Bisogno, G., Stevens, M.C.G., Meyer, W.H., Carli, M., and Anderson, J.R. (2008). Prognostic factors in metastatic rhabdomyosarcomas:

results of a pooled analysis from United States and European cooperative groups. J. Clin. Oncol. *26*, 2384-2389.

Okano, T., Yamada, N., Okuhara, M., Sakai, H., and Sakurai, Y. (1995). Mechanism of cell detachment from temperature-modulated, hydrophilic-hydrophobic polymer surfaces. Biomaterials *16*, 297-303.

Onisto, M., Slongo, M.L., Gregnanin, L., Gastaldi, T., Carli, M., and Rosolen, A. (2005). Expression and activity of vascular endothelial growth factor and metalloproteinases in alveolar and embryonal rhabdomyosarcoma cell lines. Int. J. Oncol. *27*, 791-798.

Pampaloni, F., Reynaud, E.G., and Stelzer, E.H.K. (2007). The thrid dimension bridges the gap between cell culture and live tissues. Nat. Rev. Mol. Cell Biol. *8*, 839-845

Parham, D.M. (2001). Pathologic classification of rhabdomyosarcomas and correlations with molecular studies. Mod. Pathol. *14*, 506-514.

Pavlakovic, H., Havers, W., and Schweigerer, L. (2001). Multiple angiogenesis stimulators in a single malignancy: implications for anti-angiogenic tumour therapy. Angiogenesis *4*, 259-262.

Petrie, R.J., and Yamada, K.M. (2012). At the leading edge of three-dimensional cell migration. J. Cell Sci. *125*, 5917-5926.

Pittet, P., Lee, K., Kulik, A.J., Meister, J.J., and Hinz, B. (2008). Fibrogenic fibroblasts increase intercellular adhesion strength by reinforcing individual OB-cadherin bonds. J. Cell Sci. *121*, 877-886.

Price, J.E. (2001). Xenograft models in immunodeficient animal: I. Nude mice: spontaneous and experimental metastasis models. Methods Mol. Med. *58*, 205-213.

Sawa, Y., and Miyagawa, S. (2013). Present and future perspectives on cell sheet-based myocardial regeneration therapy. BioMed Res. Int. *2013*, 583912.

Sawa, Y., Yoshikawa, Y., Toda, K., Fukushima, S., Yamazaki, K., Ono, M., Sakata, Y., Hagiwara, N., Kinugawa, K., and Miyagawa, S. (2015). Safety and efficacy of autologous skeletal myoblast sheets (TCD-51073) for the treatment of severe chronic heart failure due to ischemic heart disease. Circ. J. *79*, 991-999.

Shimizu, T., Yamato, M., Kikuchi, A., and Okano, T. (2003). Cell sheet engineering for myocardial tissue reconstruction. Biomaterials *24*, 2309-2316.

Soler, A.P., Johnson, K.R., Wheelock, M.J., and Knudsen, K.A. (1993). Rhabdomyosarcoma-derived cell lines exhibit aberrant expression of the cell-cell adhesion molecules N-CAM, N-cadherin, and cadherin-associated proteins. Exp. Cell Res. *208*, 84-93.

Sottile, J., and Hocking, D.C. (2002). Fibronectin polymerization regulates the composition and stability of extracellular matrix fibrils and cell-matrix adhesions. Mol. Biol. Cell *13*, 3546-3559.

Stupack, D.G., and Cheresh, D.A. (2002). ECM remodeling regulates angiogenesis: endothelial integrins look for new ligands. Sci. STKE *2002*, pe7.

Suzuki, R., Aruga, A., Kobayashi, H., Yamato, M., and Yamamoto, M. (2014). Development of a novel in vivo cancer model using cell sheet engineering. Anticancer Res. *34*, 4747-4754.

Thoma, C.R., Zimmermann, M., Agarkova, I., Kelm, J.M., and Krek, W. (2014). 3D cell culture systems modeling tumor growth determinants in cancer target discovery. Adv. Drug Deliv. Rev. *69-70*, 29-41.

Timmins, N.E., Dietmair, S., and Nielsen, L.K. (2004). Hanging-drop multicellular spheroids as a model of tumour angiogenesis. Angiogenesis *7*, 97-103.

Tisdale, M.J. (2004). Tumor-host interactions. J. Cell. Biochem. *93*, 871-877.

van der Worp, H.B., Howells, D.W., Sena, E.S., Porritt, M.J., Rewell, S., O'Collins, V., and Macleod, M.R. (2010). Can animal models of diseases reliably inform human studies? PLoS Med. *7*, e1000245.

van Zijl, F., Krupitza, G., and Mikulits, W. (2011). Initial steps of metastasis: cell invasion and endothelial transmigration. Mutat. Res. *728*, 23-34.

Vinci, M., Gowan, S., Boxall, F., Patterson, L., Zimmermann, M., Court, W., Lomas, C., Mendiola, M., Hardisson, D., and Eccles, S.A. (2012). Advances in establishment and analysis of three-dimensional tumor spheroid-based functional assays for target validation and drug evaluation. BMC Biol. *10*, 29.

Wang, T.Y., and Nicolson, G.L. (1983). Metastatic tumor cell invasion of brain organ tissue cultured on cellulose polyacetate strips. Clin. Exp. metastasis *1*, 327-339.

Wexler, L.H. (2015). Metastatic rhabdomyosarcoma: still room for improvement. J. Clin. Oncol. *34*, 105-106.

Wolf, K., Mazo, I., Leung, H., Engelke, K., von Andrian, U.H., Deryugina, E.I., Strongin, A.Y., Brocker, E.B., and Friedl, P. (2003). Compensation mechanism in tumor cell migration: mesenchymal-amoeboid transition after blocking of pericellular proteolysis. J. Cell Biol. *160*, 267-277.

Wrobel, E., Brzoska, E., and Moraczewski, J. (2007). M-cadherin and β-catenin participate in differentiation of rat satellite cells. Eur. J. Cell Biol. *86*, 99-109.

Xu, J., Rodriguez, D., Petitclerc, E., Kim, J.J., Hangai, M., Moon, Y.S., Davis, G.E., and Brooks, P.C. (2001). Proteolytic exposure of a cryptic site within collagen type IV is required for angiogenesis and tumor growth in vivo. J Cell Biol. *154*, 1069-1079.

Yamato, M., and Okano, T. (2004). Cell sheet engineering. Mater. Today *7*, 42-47.

Yang, J., Yamato, M., Shimizu, T., Sekine, H., Ohashi, K., Kanzaki, M., Ohki, T., Nishida,

K., and Okano, T. (2007). Reconstruction of functional tissues with cell sheet engineering. Biomaterials *28*, 5033-5043.

Yokota, J. (2000). Tumor progression and metastasis. Carcinogenesis *21*, 497-503.

Zhu, B., and Davie, J.K. (2015). New insights into signalling-pathway alterations in rhabdomyosarcoma. Br. J. Cancer *112*, 227-231.

List of publications

Original paper

1. **Li, M.,** Nagamori, E., Kino-oka, M.: Disruption of myoblast alignment by highly motile rhabdomyosarcoma cell in tissue structure. *J. Biosci. Bioeng.*, **123**, 259-264 (2017)
2. **Li, M.,** Kino-oka, M.: Degradation of endothelial network in disordered tumor-containing cell sheet. *J. Biosci. Bioeng.* http://dx.doi.org/10.1016/j.jbiosc.2017.01.017 (available online 11 March 2017).

Conferences

1. **Li, M.,** Nagamori, E., Kino-oka, M. "Evaluation of endothelial cell behavior in a multilayered myoblast sheet: as an *in vitro* angiogenesis model". Symposium on New Technology for Cell-based Drug Assay, Tokyo, Japan. December 10th, 2012.
2. **Li, M.,** Nagamori, E., Kino-oka, M. "Tumor angiogenesis model using cell sheet technology". 8th Cell Based Assay & Screening Technologies Conference, San Francisco, USA. November 6th-8th, 2013.
3. **Li, M.,** Kino-oka, M. "Highly motile rhabdomyosarcoma cell disorder of myoblast tissue via disruption of myoblast alignment". Tissue Engineering and Regenerative Medicine International Society (TERMIS)-Asia Pacific Meeting, Taiwan. September 3rd-6th, 2016.
4. **Li, M.,** Kino-oka, M. "In vitro rhabdomyosarcoma invasion model based on cell sheet technology". The 16th Congress of the Japan Society for Regenerative Medicine, Sendai, Japan. March 7th-9th, 2017.

Poster award

Student & Young Investigator Section Poster Award, 2nd Place. Tissue Engineering and Regenerative Medicine International Society (TERMIS)-Asia Pacific Meeting, Taiwan. September 3rd-6th, 2016.

Acknowledgements

This study was carried out from 2011 to 2017 at the Department of Biotechnology, Graduate School of Engineering, Osaka University.

First and foremost, I would like to express my deepest gratitude to my supervisor Prof. Masahiro Kino-oka, for providing me with the opportunity to study at Osaka University as a PhD student. His patience, motivation and immense knowledge helped me conquer the difficulties that were impossible to do by myself.

I am very grateful to Associate Prof. Eiji Nagamori who is the leader of the group I belonged to, instructed me expertisely, understandably and patiently. My sincere gratefulness would like to express to Associate Prof. Mee-Hae Kim, her comments and suggestions helped me to achieve more in my research.

I would like to express great thanks to Prof. Kazuhito Fujiyama and Prof. Takeshi Omasa for their constructive comments and precious time on reviewing this thesis.

Thanks are given to all my group members, especially to Assistant Prof. Kei Kanie, Dr. Ngo Xuan Trung, Dr. Yihua Cao, Mr. Masashi Oda and Ms. Yingzi Zhao for their help to initiate this study, and Mr. Tadashi Nakamura for his continuous help along the whole period of this study. I also want to thank all the other members of Kino-oka laboratory for their help and collaboration.

I greatly appreciate all international students in my batch, especially Ms. Brit Gracy David and Ms. Emilda Teresa Gomez for their friendship and encouragement. I also want to thank all the friends I met in Japan, for their help and encouragement.

I am very grateful to the Japanese Government for the financial support through the Monbukagakusho Scholarship during my study in Japan.

Last but not least, I would like to thank my family for their understanding and supporting. The love and encouragement from them are the resource of power which keep me moving forward.

Menglu Li